Supporting Information

Simple Organic Donors Based on Halogenated Oligothiophenes for All Small Molecule Solar Cells with Efficiency Over 11%

Tainan Duan[+], Jie Gao[+], Tongle Xu, Zhipeng Kan, Wenjing Chen, Ranbir Singh[*], Gururaj P. Kini, Cheng Zhong[*], Donghong Yu, Zhengguo Xiao, Zeyun Xiao and Shirong Lu[*]

Content:

1. General Experimental Details

All reactions were performed under nitrogen atmosphere and solvents were purified and dried from appropriate drying agents using standard techniques prior to use. Reagents available from commercial sources were used without further purification unless otherwise stated. Flash chromatography was performed by using Silicycle Silica Flash P60 (particle size 40-63 μm, 60 Å, 230-400 mesh) silica gel. Silica gel on TLC-PET foils from Fluka was used for TLC. Recycling SEC in THF or ethanol-stabilized chloroform was carried out through a set of two JAIGEL-4H-40 preparative SEC columns mounted on an LC-9130NEXT (JAI) system equipped with coupled UV-254NEXT and RI-700NEXT detectors. All compounds were characterized by NMR spectroscopy on Bruker Avance III Ultrashield Plus instruments (600 MHz). The spectra were referenced on the internal standard TMS. High-resolution mass spectrometry (HRMS) data of 2F7T and 2Cl7T was recorded using a Bruker solariX 70 FT-MS. Note: Spectroscopy-grade $CHCl_3$ was filtered through basic alumina prior to use in order to suppress solvent acidity and avoid undesired protonation reactions that may influence the spectral absorption of the molecular acceptors described in this study.

2. Synthetic Protocols and Characterizations

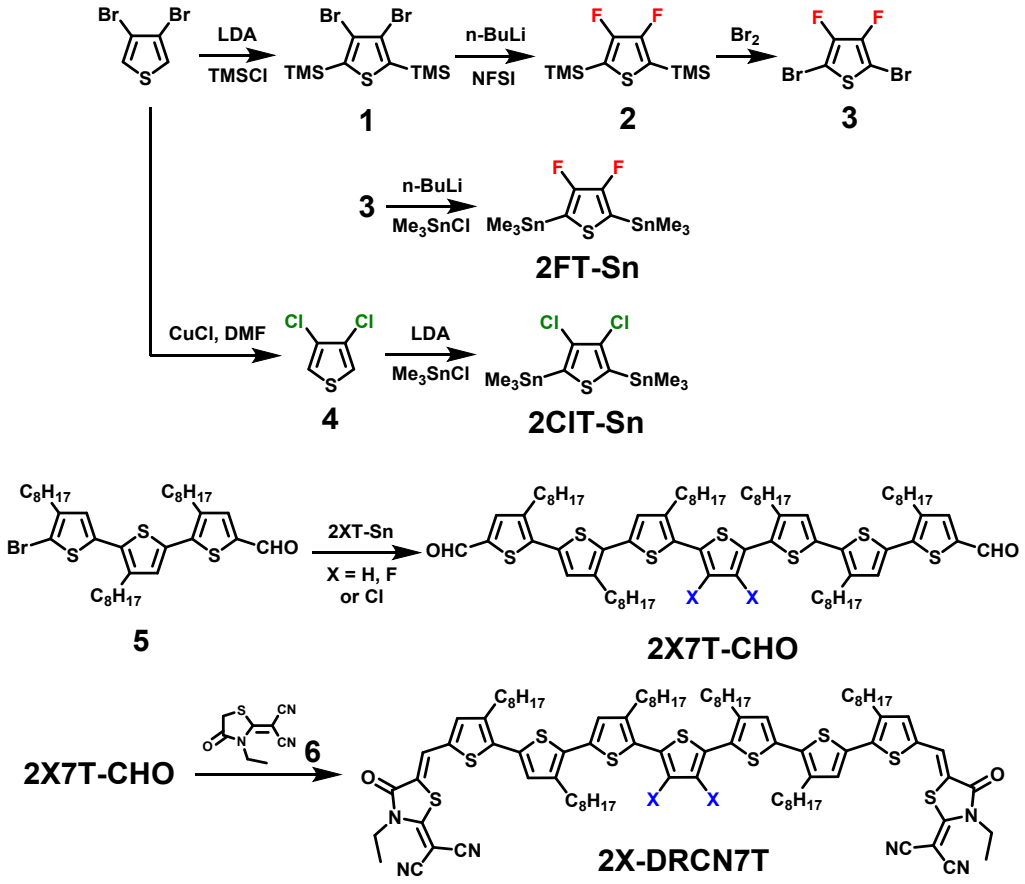

Scheme S1. Synthesis of the donors **2X7T**.

Note: Compounds **2FT-Sn**[1] and **5**[2-3] were prepared according to previously report procedures.

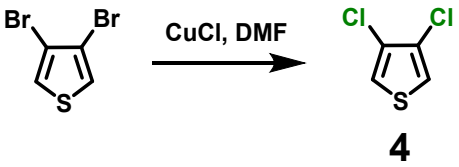

3,4-dichlorothiophene (4): Dichlorothiophene was synthesized according to previous report with minor modification. To a rigorously stirred solution of 3,4-dibromothiophene (4.84 g, 20.0 mmol) in 120 mL DMF, anhydrous CuCl (5.94 g, 60.0 mmol) was added in one portion. Then the mixture was heated to reflux and stirred for 24 h. After cooling down to room temperature, the resulting suspension was filtered. The filtrate was washed with saturated NaCl solution (200 mL) and then extracted with acetyl acetate (3 × 50 mL). The organic phase was combined, dried

over Na_2SO_4, filtered, and concentrated under reduced pressure. The crude product was firstly passed through a flash column (PE as eluent), then subjected to vacuum distillation to yield pure 3,4-dichlorothiophene as a colorless oil (2.87 g, yield: 94%). ^{1}H NMR (600 MHz, $CDCl_3$, δ ppm): 7.20 (s, 2H). ^{13}C NMR (150 MHz, $CDCl_3$, δ ppm): 124.98, 120.68.

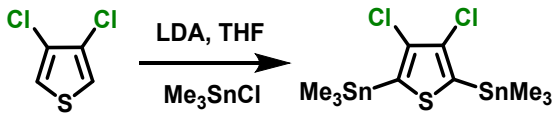

2ClT-Sn

(3,4-dichlorothiophene-2,5-diyl)bis(trimethylstannane) (2ClT-Sn): In a pre-dried Schlenk tube, a solution of 3,4-dichlorothiophene (1.53 g, 10.0 mmol) in anhydrous THF (40 mL) was cooled to -78 °C. A solution of LDA (2.0 M in THF, 11.0 mL, 22.0 mmol) was added dropwise, and the mixture was stirred for 2 h at -78 °C. Next, trimethyltin chloride in THF (1.0 M, 24.0 mL, 24.0 mmol) was added to the mixture in one portion. The cooling bath was then removed, the mixture was allowed to warm to room temperature, and was stirred overnight. The reaction was quenched with saturated KF solution (100 mL) and the aqueous phase was extracted with dichloromethane (2 × 50 mL). The organic phase was collected, dried over Na_2SO_4, concentrated under reduced pressure, and compound **2ClT-Sn** was obtained as a pale yellow solid used in the next step without the need for further purification (4.40 g, yield: 92%). ^{1}H NMR (600 MHz, CD_2Cl_2, δ ppm): 0.34 (s, 18H). ^{13}C NMR (150 MHz, CD_2Cl_2, δ ppm): 139.10, 131.67, -8.79.

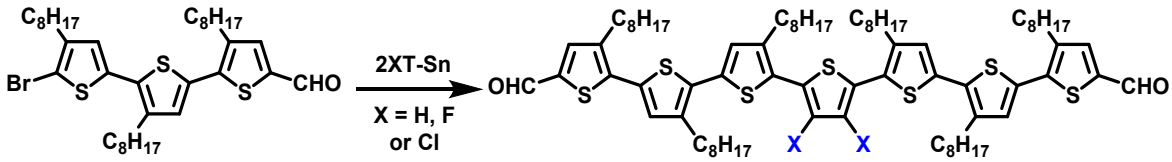

5 **2X7T-CHO**

General procedure for the preparation of the aldehyde 2X7T-CHO (X = H, F or Cl): In a pre-dried Schlenk tube, **2XT-Sn** (1.0 equiv.), 5''-bromo-3,4',4''-trioctyl-[2,2':5',2''-terthiophene]-5-carbaldehyde (**5**) (2.2 equiv.) and $Pd(PPh_3)_4$ (0.08 equiv.) were dissolved in pre-degassed toluene (30 mL). The recation mixture was heated to 110 °C and was stirred for 48 h. Next, the mixture was concentrated under reduced pressure. The crude product was purified by column

chromatography over SiO_2 using hexanes/CH_2Cl_2 (1:1) as the eluent. The solvent was removed by rotary evaporation, affording desired compound **2X7T-CHO**.

3''',4'''-difluoro-3,3'''',3''''',3''''''',4',4''-hexaoctyl-[2,2':5',2'':5'',2''':5''',2'''':5'''',2''''':5''''',2'''''':5'''''',2''''''-sepithiophene]-5,5''''''-dicarbaldehyde (2F7T-CHO): Red solid (430 mg, 87%). ^{1}H NMR (600 MHz, $CDCl_3$, δ ppm): 9.85 (s, 2H), 7.62 (s, 2H), 7.16 (s, 2H), 7.07 (s, 2H), 2.86-2.74 (m, 12H), 1.72-1.71 (m, 12H), 1.44-1.31 (m, 60H), 0.90-0.89 (m, 18H). ^{13}C NMR (150 MHz, $CDCl_3$, δ ppm): 182.35, 142.94, 142.49, 142.35, 140.96, 140.73, 140.67, 140.59, 140.46, 140.32, 138.82, 136.06, 133.09, 132.33, 130.46, 128.47, 124.50, 112.87, 112.84, 112.80, 112.77, 31.86, 31.84, 30.49, 30.26, 29.52, 29.49, 29.47, 29.44, 29.41, 29.39, 29.38, 29.36, 29.23, 29.21, 22.64, 14.04. ^{19}F NMR (565 MHz, $CDCl_3$, δ ppm): -132.58.

3''',4'''-dichloro-3,3'''',3''''',3''''''',4',4''-hexaoctyl-[2,2':5',2'':5'',2''':5''',2'''':5'''',2''''':5''''',2'''''':5'''''',2''''''-sepithiophene]-5,5''''''-dicarbaldehyde (2Cl7T-CHO): Orange solid (418 mg, 84%). ^{1}H NMR (600 MHz, $CDCl_3$, δ ppm): 9.83 (s, 2H), 7.59 (s, 2H), 7.13 (s, 2H), 7.07 (s, 2H), 2.84-2.79 (m, 8H), 2.67 (t, J = 7.2 Hz, 4H), 1.70-1.64 (m, 12), 1.41-1.28 (m, 60H), 0.89-0.87 (m, 18). ^{13}C NMR (150 MHz, $CDCl_3$, δ ppm): 182.46, 144.19, 141.01, 140.66, 140.46, 140.26, 138.95, 136.64, 133.05, 132.37, 130.48, 128.86, 127.96, 125.78, 124.14, 31.88, 31.86, 30.54, 30.52, 30.27, 29.53, 29.45, 29.44, 29.40, 29.38, 29.34, 29.26, 29.24, 22.66, 14.09.

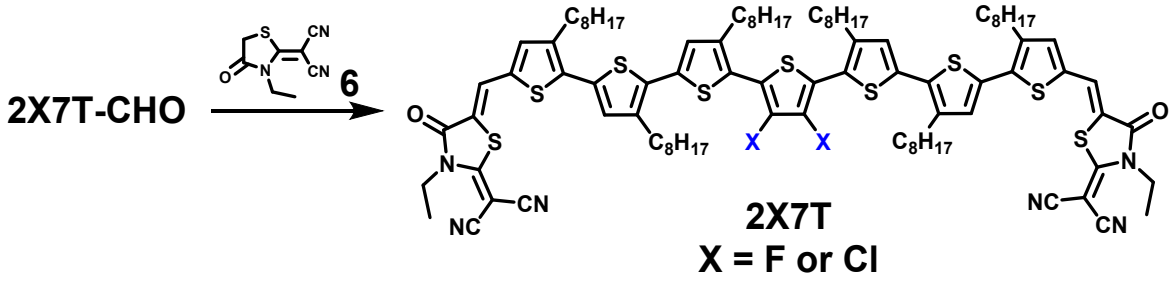

General procedure for the preparation of the molecular donors 2F7T and 2Cl7T: The aldehyde **2X7T-CHO** (1.0 equiv.), 2-(3-ethyl-4-oxothiazolidin-2-ylidene)malononitrile (**6**, 4.0 equiv.) and ammonium acetate (0.1 equiv.) were added into a mix solution of chloroform/acetic acid (5 mL/20 mL), and the mixture was heated to 100 °C and stirred for 24 h. The reaction mixture was allowed to cool down to room temperature, was filtered, and washed with methanol

(2 × 20 mL) and ethyl acetate (2 × 20 mL), affording the desired products in high yield and high purity. Further purification can be simply performed via recrystallization in ethyl acetate. (**2F7T** or **2Cl7T**)

2,2'-((5Z,5'Z)-((3''',4'''-difluoro-3,3'''',3''''',3''''''',4',4''-hexaoctyl-[2,2':5',2'':5'',2''':5''',2'''':5'''',2''''':5''''',2'''''':5'''''-sepithiophene]-5,5''''''-diyl)bis(methanylylidene))bis(3-ethyl-4-oxothiazolidine-5,2-diylidene))dimalononitrile (2F7T): Purple-black solid (110 mg, 93%). ^{1}H NMR (600 MHz, $CHCl_3$, δ ppm): 8.00 (s, 2H), 7.30 (s, 2H), 7.19 (s, 2H), 7.08 (s, 2H), 4.34 (m, 4H) 2.85-2.81 (m, 8H), 2.75 (t, J = 7.2 Hz, 4H), 1.72-1.68 (m, 12H), 1.42-1.28 (m, 60H), 0.87 (m, 18H). ^{13}C NMR(150 MHz, $CHCl_3$, δ ppm): 165.90, 165.59, 142.97, 141.40, 140.94, 140.88, 138.83, 135.94, 133.84, 132.71, 132.57, 130.62, 128.63, 128.52, 124.62, 113.48, 113.31, 112.28, 55.61, 40.67, 31.88, 31.85, 30.64, 30.54, 30.19, 29.61, 29.57, 29.49, 29.45, 29.42, 29.39, 29.37, 29.30, 29.27, 29.24, 22.67, 14.19, 14.09. ^{19}F NMR (565 MHz, $CDCl_3$, δ ppm): -132.51.

2,2'-((5Z,5'Z)-((3''',4'''-dichloro-3,3'''',3''''',3''''''',4',4''-hexaoctyl-[2,2':5',2'':5'',2''':5''',2'''':5'''',2''''':5''''',2'''''':5'''''-sepithiophene]-5,5''''''-diyl)bis(methanylylidene))bis(3-ethyl-4-oxothiazolidine-5,2-diylidene))dimalononitrile (2Cl7T): Purple-blue solid (98 mg, 90%). ^{1}H NMR (600 MHz, $CHCl_3$, δ ppm): 8.00 (s, 2H), 7.30 (s, 2H), 7.19 (s, 2H), 7.10 (s, 2H), 4.34 (m, 4H) 2.84-2.83 (m, 8H), 2.67 (br, 4H), 1.74-1.64 (m, 12H), 1.43-1.28 (m, 60H), 0.88-0.86 (m, 18H). ^{13}C NMR(150 MHz, $CHCl_3$, δ ppm): 165.91, 165.59, 144.26, 141.42, 140.95, 140.88, 138.82, 136.56, 133.85, 132.75, 132.57, 130.63, 128.84, 128.64, 128.04, 125.89, 124.17, 113.49, 113.31, 112.28, 55.62, 40.67, 31.88, 31.85, 30.65, 30.58, 30.20, 29.63, 29.49, 29.46, 29.40, 29.39, 29.36, 29.30, 29.24, 22.66, 14.20, 14.09.

3. Thermogravimetric Analysis (TGA)

Thermogravimetric Analysis (TGA) was performed with a Mettler-Toledo TGA/DSC 3+ analyzer under a nitrogen atmosphere, using aluminum crucibles.

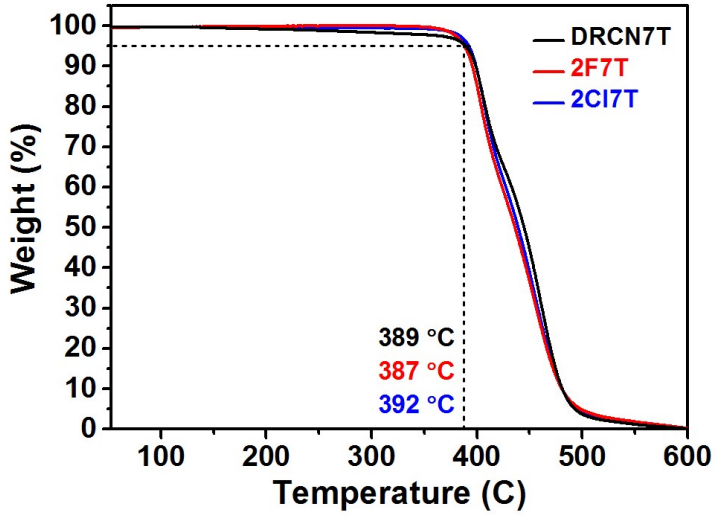

Figure S1. Thermogravimetric analyses (TGA) of **2F7T**, **2Cl7T** and **DRCN7T**. The molecular acceptors show high thermal-stability under nitrogen atmosphere; *ca.* 5% weight loss observed at 396 °C and 409 °C, respectively.

4. Density Functional Theory (DFT) Calculations

The density functional theory (DFT) calculations were performed at the ω-tuned wb97x/def2TZVP level based on PBE0-D3BJ/def2-SVP optimized geometry with the Gaussian 09 (Revision E.01) code. The small-molecule side chains were modeled as methyl groups; while side chains play an important role in the organization of small molecules and polymers in the solid state, these have only marginal influence on the electronic and optical properties of the single isolated small-molecule/polymer chain in the gas phase. The direction and magnitude of dipole moments are shown in Figure S1. The σ acceptor ability of F increase the dipole moments while the π donor ability of Cl decrease the dipole moments. The HOMO and LUMO distributions are shown in Figure S2. For all three donors, the LUMOs are delocalized over the whole molecule and HOMOs are mainly localized over the centrol poly-thiophene moiety. The 2Cl7T has more HOMO distribution on Cl atom, compared with HOMO distribution on F atom in 2F7T.

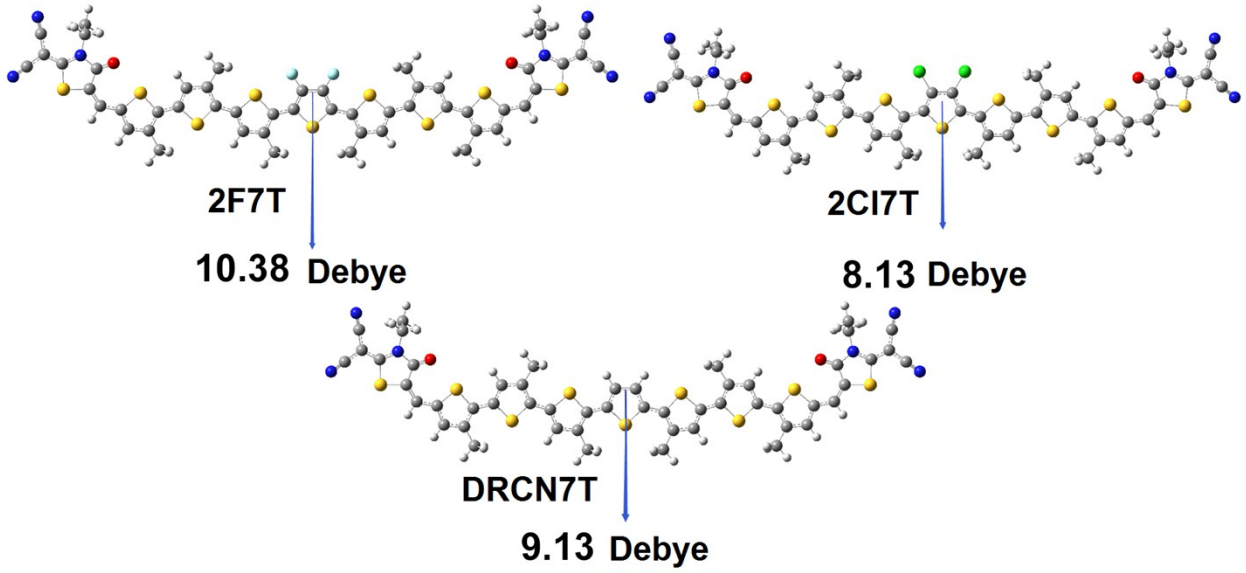

Figure S2. Optimized geometries with dipole moments for three oligohiophene molecules.

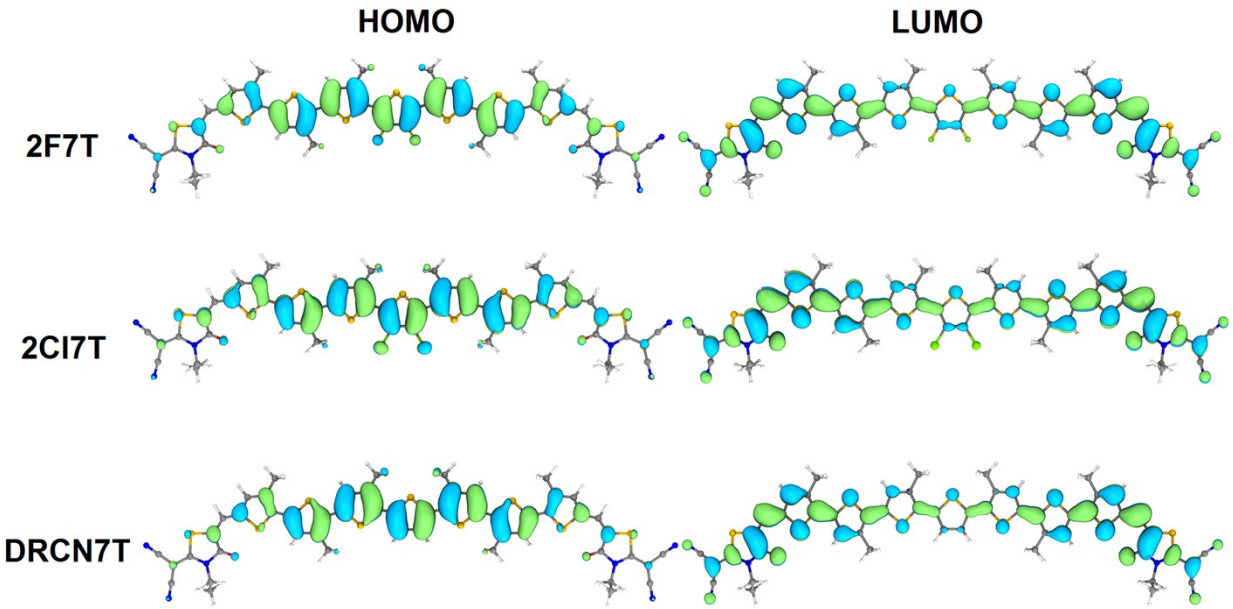

Figure S3. HOMO-LUMO distribution of three donors.

5. UV-Vis Spectroscopy

Temperature-dependent UV-Vis spectra in solution were recorded on a PerkinElmer LAMBDA 365 UV-Vis spectrophotometer.

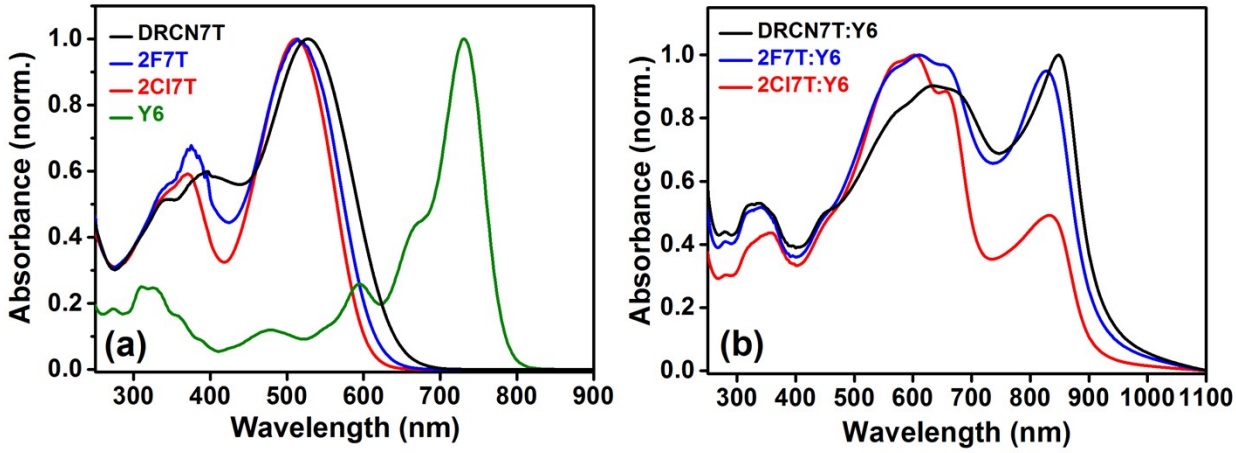

Figure S4. **(a)** Normalized UV-vis spectra of SM donors and acceptor in chloroform solution. **(b)** Normalized UV-Vis absorption spectra of optimized bulk-heterojunction SM donor:Y6 blend films.

6. Cyclic Voltammogram and Energy Level Diagram

Electrochemical measurements were performed with a CIH660e electrochemical workstation, using a glassy carbon button electrode as the working electrode, a platinum wire as the auxiliary electrode, and a Ag/Ag^+ glass electrode as the reference electrode. The Ag/Ag^+ reference electrode was calibrated using the ferrocene/ferrocenium (Fc/Fc^+) redox couple. Fc/Fc^+ is taken to be 4.8 eV relative to the vacuum level. [3]

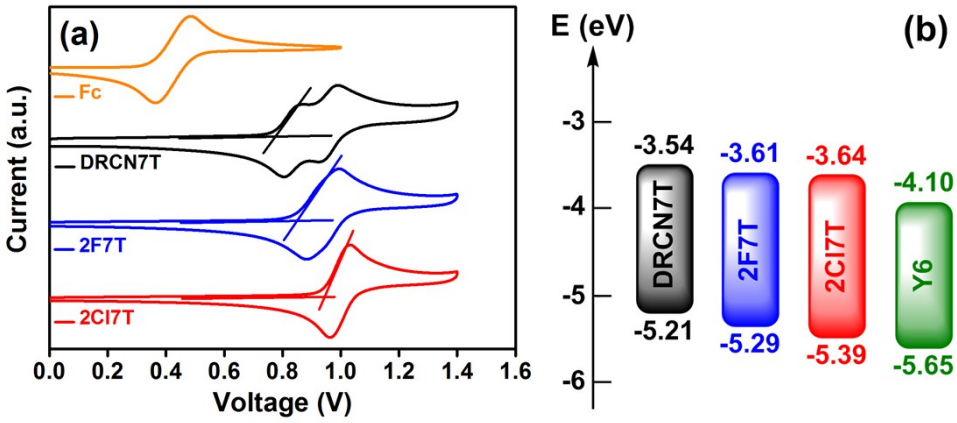

Figure S5. **(a)** Oxidation scans of the SM donor DRCN7T, **2F7T** and **2Cl7T**; vs. Fc/Fc_+. (b) Energy level diagram of SM donors and SM acceptor used in this work.

Table S1. Summary of electrochemical parameters of the SM donors.

SM donors	$E_{onset,ox}$[a] [V]	λ_{onset} [nm]	E_{opt}[b] [V]	HOMO[c] (eV)	LUMO[d] (eV)
DRCN7T	0.77	742	1.67	-5.21	-3.54
2F7T	0.85	738	1.68	-5.29	-3.61
2Cl7T	0.95	708	1.75	-5.39	-3.64

[a] Onset oxidation potentials of SM donors; [b] E_{opt} is derived from the absorption onset of the SM donor neat film: $E_{opt} = 1240/\lambda_{onset}$; [c] $E_{HOMO} = -[E_{onset,\,ox} + (4.8 - E_{Fc/Fc+})]$ eV; [d] $E_{LUMO} = (E_{HOMO} + E_{opt})$ eV

7. Differential Scanning Calorimetry (DSC) Measurements

Differential Scanning Calorimetry (DSC) measurements were performed on a Mettler-Toledo TGA/DSC 3+ analyzer under a nitrogen atmosphere, using aluminum crucibles.

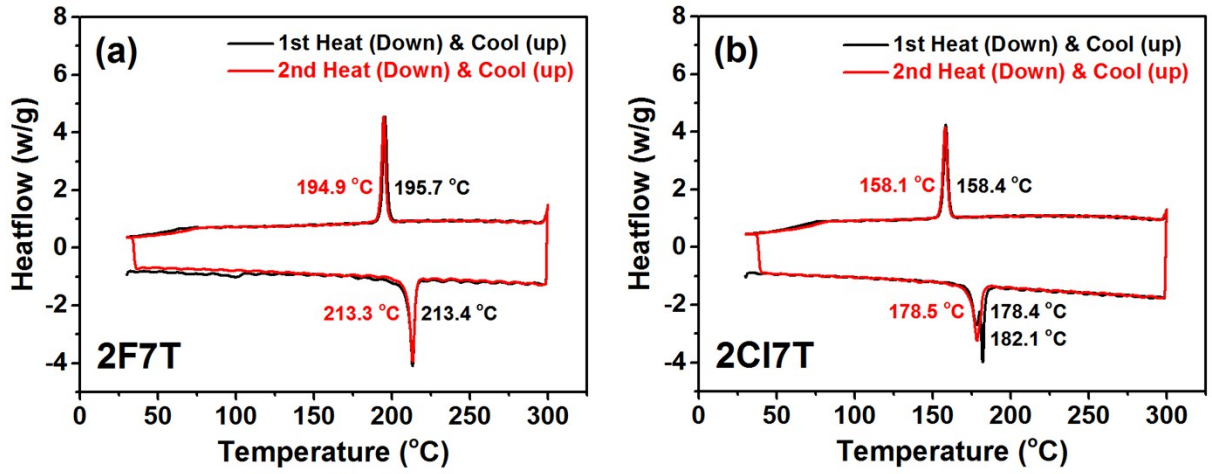

Figure S6. Differential Scanning Calorimetry (DSC) traces of (a) **2F7T** and (b) **2Cl7T**. Analyses carried out with a scan rate of 10 °C/min between 30 °C and 300 °C. Two SM donors show an apparent phase transition around 213 °C and 178 °C, respectively, suggesting a melt transition in light of the presence of a first order solidification peak on the cooling scan.

8. Device Fabrication

The BHJ solar cells were prepared on the glass substrates with tin-doped indium oxide (ITO , 15Ω/sq) on part of the surface and the effective area of each device is 0.11cm^2. The entire cleaning process of the substrates can be divided into four sections. At first, the substrates were prewashed with detergent in a Ultrasonic cleaning machine for 15 min to remove the stains. Then deionized water was used to wash the detergent left on the substrates. Followed by this, the substrates were cleaned by acetone for 15 min in the ultrasonic bath. At last, isopropanol was applied to remove organic residues before immersing in an ultrasonic bath for 15 min. Next, the samples were dried with pressurized nitrogen before being exposed to a UV-ozone plasma for 20 min. A thin layer (~35nm) of PEDOT:PSS was spin cast onto the UV-treated samples, dried on the hot plate at 160 °C for 15 minutes, and then transferred into a dry nitrogen glovebox (< 3 ppm O_2).

All solutions were prepared in a glovebox using 2Cl7T, 2F7T and DRCN7T synthesized and Y6 purchased from derthon. Optimized devices were obtained by dissolving the small molecules and Y6 in chloroform. The as-prepared solutions were stirred 3 hours at 40 °C before being cast. The effects of various solution concentrations, blend ratios and different post-conditions such as TA, SVA and combination of this two methods on the device performance were also examined. The active layers were spin-cast from the solutions at 40 °C at an optimized speed of 6000 rpm for 2Cl7T, 4000 rpm for 2F7T and 3000 rmp for DRCN7T in a time period of 30 s, using a programmable spin coater, resulting in films of 110nm, 104nm and 120 nm in thickness respectively.

Next, the samples were dealt with corresponding optimized conditions. For 2Cl7T:Y6, the samples were exposed to CF solvent steam for 25s followed by TA at 120min for 10 min. As to 2F7T:Y6, samples were heated on a temperature of 130°C for 10 min. Meanwhile, DRCN7T:Y6 samples were placed on a hot plate with 20 °C for 10 min. After that, PFNBr solution were spin cast onto the samples at a speed of 3000 rmp during a period of 30 s. 100 nm of Ag electrodes evaporated at 0.3 Å s^{-1} during the former 100 Å period and then evaporated at 22 Å s^{-1} , pressure of less than 2×10^{-6} Torr. Following electrode deposition, samples underwent *J-V* testing.

9. Additional PV Device Performance Data

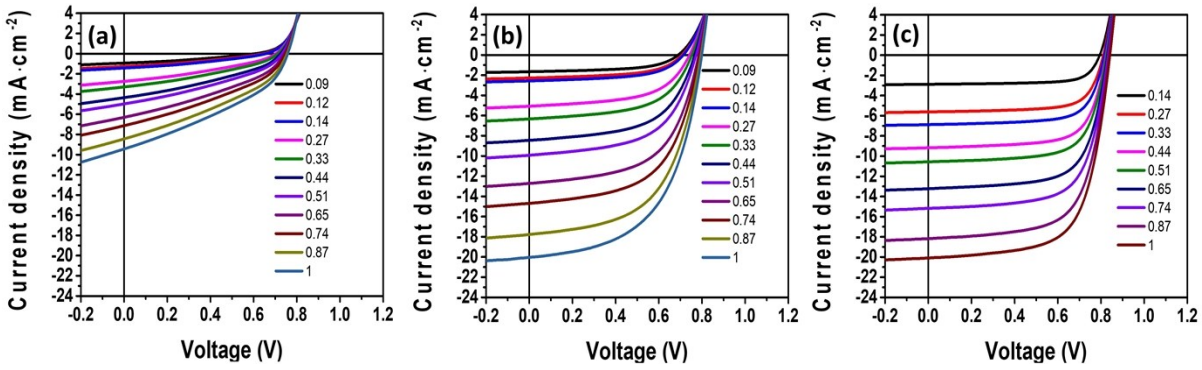

Figure S7. *J-V* curves of BHJ solar cells made with **(a) DRCN7T, (b) 2F7T** and **(c) 2Cl7T** under different light intensities.

Table S2. Donor-Acceptor ratio dependence and concentration dependence for 2Cl7T:Y6 devices with 4k rmp and TA at 110°C for 10min treatment. Performance includes standard deviation across at least 10 devices.

Con	D/A ratio (wt:wt)	V_{OC} (V)	J_{SC} (mA/cm^2)	FF (%)	PCE (%)	MAX PCE (%)
20	1.5:1	0.84(±0.01)	18.89(±0.05)	64.45(±0.75)	10.17(±0.03)	10.47
	1:1	0.84(±0.01)	18.29(±0.17)	61.68(±1.69)	9.49(±0.42)	9.91
	1:1.5	0.84(±0.01)	16.75(±0.09)	62.81(±1.46)	8.85(±0.22)	9.08
15	1.5:1	0.84(±0.00)	16.83(±0.13)	67.11(±0.87)	9.47(±0.18)	9.66
	1.8:1	0.85(±0.00)	17.26(±0.02)	67.68(±1.15)	9.88(±0.18)	10.06
	2:1	0.85(±0.00)	18.10(±0.09)	68.12(±0.14)	10.45(±0.07)	10.52
18	2:1	0.84(±0.00)	18.12(±0.14)	68.40(±2.08)	10.47(±0.44)	10.91
	2.3:1	0.85(±0.00)	17.88(±0.29)	65.45(±0.57)	9.92(±0.25)	10.17

Table S3. Donor-Acceptor Thickness dependence for 2Cl7T:Y6 devices with TA at 110°C for 10 min treatment. Performance includes standard deviation across at least 10 devices.

Con	D/A ratio (wt:wt)	Rs (rmp)	V_{OC} (V)	J_{SC} (mA/cm^2)	FF (%)	PCE (%)	MAX PCE (%)
18	2:1	3k	0.84(±0.01)	17.79(±0.00)	68.30(±1.90)	10.19(±0.37)	10.56
		4k	0.85(±0.00)	18.26(±0.34)	67.89(±0.07)	10.48(±0.21)	10.69
		5k	0.85(±0.00)	18.57(±0.04)	68.58(±0.03)	10.79(±0.08)	10.87
		6k	0.84(±0.01)	18.20(±0.06)	69.20(±1.28)	10.59(±0.32)	10.91
15	2:1	1k	0.85(±0.00)	17.01(±0.07)	65.34(±2.43)	9.40(±0.41)	9.81

Table S4. Diverse post-condition dependence for 2Cl7T:Y6 devices with concentration of 18mg/ml, D/A ratio (wt:wt) 2:1 and active layer for 6k rmp. Performance includes standard deviation across at least 10 devices.

Con	Treatment	V_{OC} (V)	J_{SC} (mA/cm^2)	FF (%)	PCE (%)	MAX PCE (%)
18	TA 110 °C 10 min	0.85(±0.00)	18.10(±0.09)	68.12(±0.14)	10.45(±0.07)	10.52
	TA 120 °C 10 min	0.84(±0.00)	18.64(±0.63)	68.40(±0.39)	10.67(±0.30)	10.97
	TA 130 °C 10 min	0.84(±0.00)	17.62(±0.07)	67.94(±1.95)	10.02(±0.32)	10.35
	SVA(CF, 20 sec)+TA[a]	0.83(±0.01)	19.69(±0.41)	68.15(±1.97)	11.19(±0.26)	11.45
	TA+SVA(CF, 20 sec)[b]	0.82(±0.01)	18.03(±0.00)	61.88(±0.65)	9.17(±0.15)	9.33

[a] SVA (chloroform, 20 sec) followed by TA (120 °C, 10 min). [b] TA (120 °C, 10 min) followed by SVA (chloroform, 20 sec).

Table S5. Donor-Acceptor ratio dependence and concentration dependence for 2F7T:Y6 devices with TA at 110°C for 10min treatment. Performance includes standard deviation across at least 10 devices.

Con	D/A ratio (wt:wt)	V_{OC} (V)	J_{SC} (mA/cm2)	FF (%)	PCE (%)	MAX PCE (%)
20	1:1.2	0.83(±0.00)	13.73(±0.81)	43.85(±0.62)	5.00(±0.35)	5.35
	1:1	0.81(±0.00)	17.49(±0.17)	47.69(±1.04)	6.79(±0.24)	7.03
	1.2:1	0.82(±0.01)	18.45(±0.18)	54.26(±1.84)	8.20(±0.28)	8.48
	1.5:1	0.82(±0.01)	17.31(±0.03)	53.25(±1.13)	7.55(±0.25)	7.80

Table S6. Diverse post-condition dependence for 2F7T:Y6 devices with the D/A ratio (wt:wt) 1.2:1. Performance includes standard deviation across at least 10 devices.

Con	Treatment	V_{OC} (V)	J_{SC} (mA/cm2)	FF (%)	PCE (%)	MAX PCE (%0
20	TA 110 °C 10min	0.82(±0.01)	18.45(±0.18)	54.26(±1.84)	8.20(±0.28)	8.48
	TA 120 °C 10min	0.78(±0.00)	19.31(±0.15)	51.07(±1.12)	7.74(±0.13)	7.87
	TA 130 °C 10min	0.79(±0.01)	20.89(±0.55)	54.13(±0.70)	8.93(±0.48)	9.41

Table S7. Data for DRCN7T:Y6 devices with the D/A ratio (wt:wt) 1:1. Performance includes standard deviation across at least 10 devices.

Con	Treatment	V_{OC} (V)	J_{SC} (mA/cm2)	FF (%)	PCE (%)	MAX PCE (%)
20	TA 120 °C 10min	0.76(±0.01)	8.44(±0.12)	36.48(±1.35)	2.33(±0.16)	2.48

10. Carrier Mobility Measurements

The carrier mobility (hole and electron mobility) of photoactive active layer was obtained by fitting the dark current of hole/electron-only diodes to the space-charge-limited current (SCLC) model. Hole-only diode configuration: Glass/ITO/PEDOT:PSS/active layer/MoO_3/Ag; here, V_{bi} = 0 V (flat band pattern formed by PEDOT:PSS-MoO_3). Electron-only diode configuration: Glass/ITO/ZnO/ /active layer/DPO/Ag; here, V_{bi}=0.5V was used following the protocol reported.[3] The active layer thickness was determined by a Tencor surface profilometer. The electric-field dependent SCLC mobility was estimated using the following equation:

$$J(V) = \frac{9}{8}\varepsilon_0\varepsilon_r\mu_0 exp\left(0.89\beta\sqrt{\frac{V - V_{bi}}{L}}\right)\frac{(V - V_{bi})^2}{L^3}$$

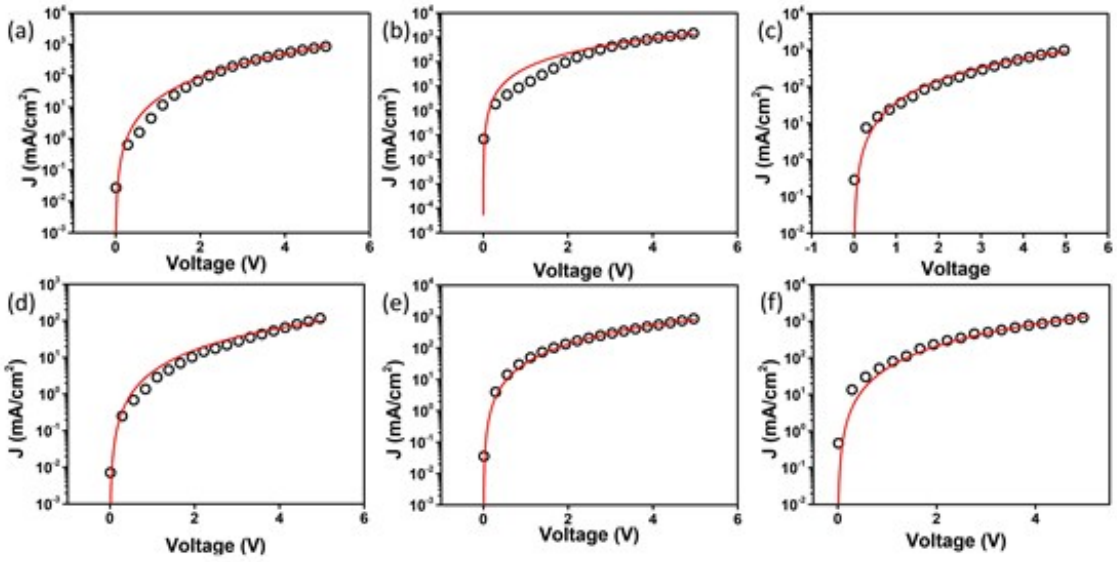

Figure S8. (a)(b)(c) are the electron mobility fitting examples of DRCN7T, 2F7T and 2Cl7T, respectively. (d)(e)(f) are the hole mobility fitting examples of DRCN7T, 2F7T and 2Cl7T, respectively.

Table S8. Average mobility values of devices of DRCN7T:Y6, 2F7T:Y6, and 2Cl7T:Y6.

System	μ_e($cm^2V^{-1}s^{-1}$)	μ_h($cm^2 V^{-1}s^{-1}$)
DRCN7T:Y6	3.73×10^{-4}	4.50×10^{-4}
2F7T:Y6	2.2×10^{-4}	2.59×10^{-4}
2Cl7T:Y6	1.96×10^{-4}	2.88×10^{-4}

11. Carrier Recombination Analysis

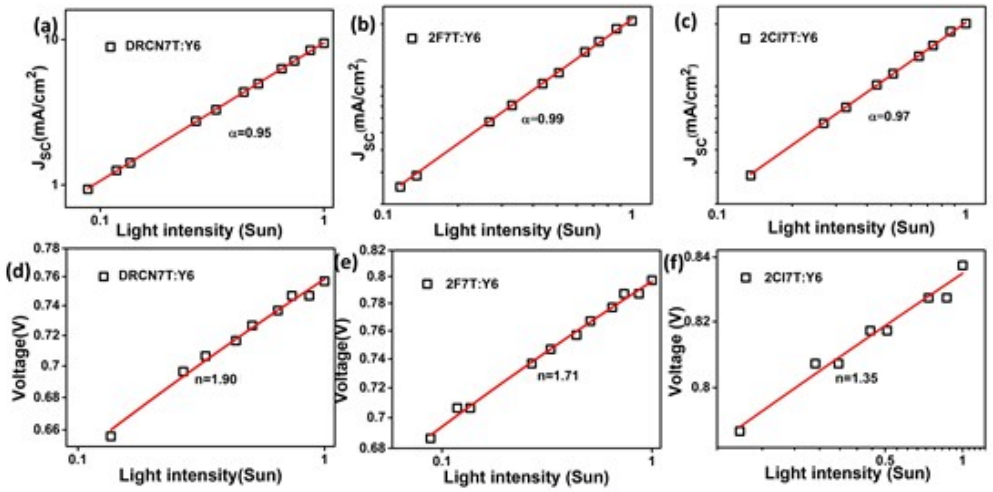

Figure S9. J_{SC} vs. light intensity for optimized (a) DRCN7T:Y6, (b) 2F7T:Y6 and (c) 2Cl7T:Y6. The solid lines correspond to the fits derived from the expression $J_{SC} \propto I^{\alpha}$. With α=0.95±0.01, α=0.99±0.02 and α=0.97±0.02 for DRCN7T:Y6, 2F7T:Y6 and 2Cl7T:Y6 respectively. Note: bimolecular recombination is not the main limiting factor suppressing efficiency for the optimized blends.

V_{OC} vs. light intensity for optimized (d) DRCN7T:Y6 (e) 2F7T:Y6 and (f)2Cl7T:Y6. The solid lines corresponding to the fits derived from the expression $V_{OC} \propto n\frac{kT}{q}ln(I)$. With n=1.90±0.07, n=1.71±0.04 and n=1.35±0.06 for DRCN7T:Y6, 2F7T:Y6 and 2Cl7T:Y6 respectively.

12. Transmission Electron Microscopy (TEM) Imaging

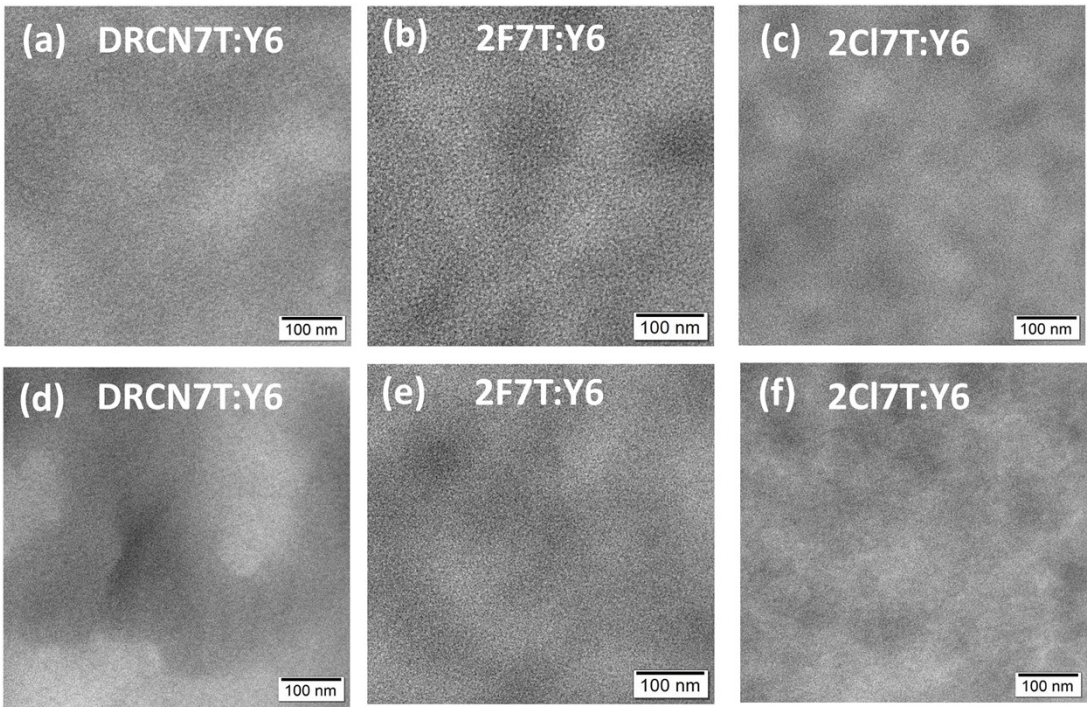

Figure S10. Morphology analyses of "as-cast" and "optimized" BHJ active layers with SM donors and Y6 acceptor. **(a, d)** DRCN7T:Y6 **(b, e)** 2F7T:Y6 **(c, f)** 2Cl7T:Y6 **.** Scale bar: 100nm.

13. Atomic Force Microscopy (AFM) Imaging

A 5400 Agilent Atomic Force Microscope (AFM) was used to image the active layers in tapping mode (topography and phase images).

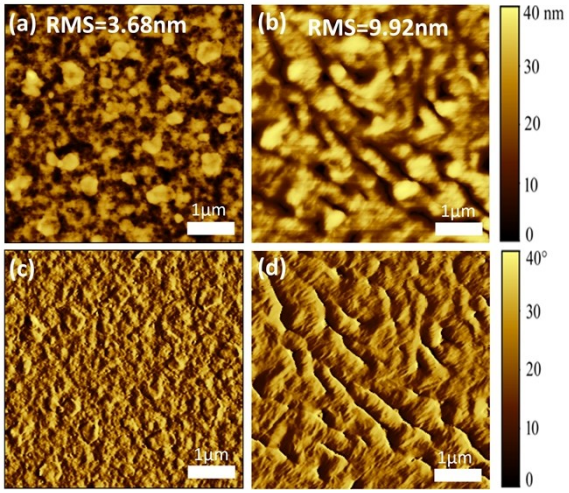

Figure S11. Topography and phase images of thin films of DRCN7T:Y6. Topography images of a) and b)DRCN7T:Y6 without and with post-condition. Phase images of c) and d) DRCN7T:Y6 without and with post-condition. Scale bar is 1 μm.

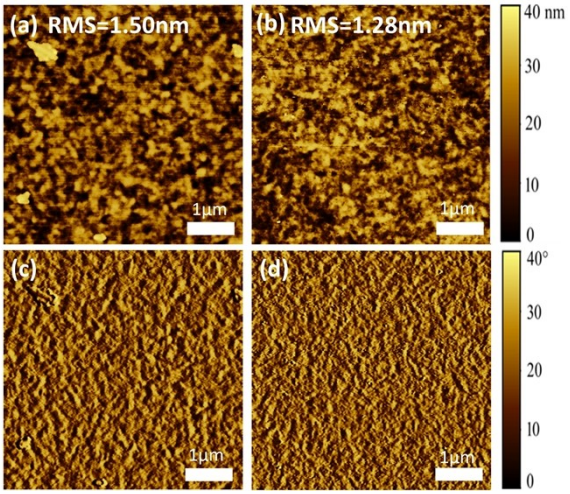

Figure S12. Topography and phase images of thin films of 2F7T:Y6. Topography images of a) and b) 2F7T:Y6 without and with post-condition. Phase images of c) and d) 2F7T:Y6 without and with post-condition. Scale bar is 1 μm.

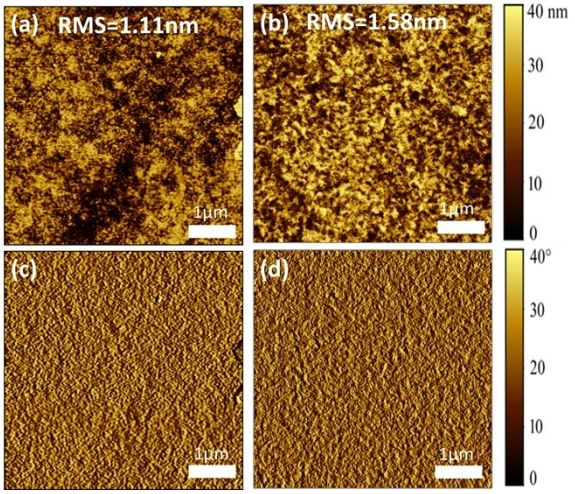

Figure S13. Topography and phase images of thin films of 2Cl7T:Y6. Topography images of a) and b) 2Cl7T:Y6 without and with post-condition. Phase images of c) and d) 2Cl7T:Y6 without and with post-condition. Scale bar is 1 μm.

14. Photoluminescence Spectroscopy (PL)

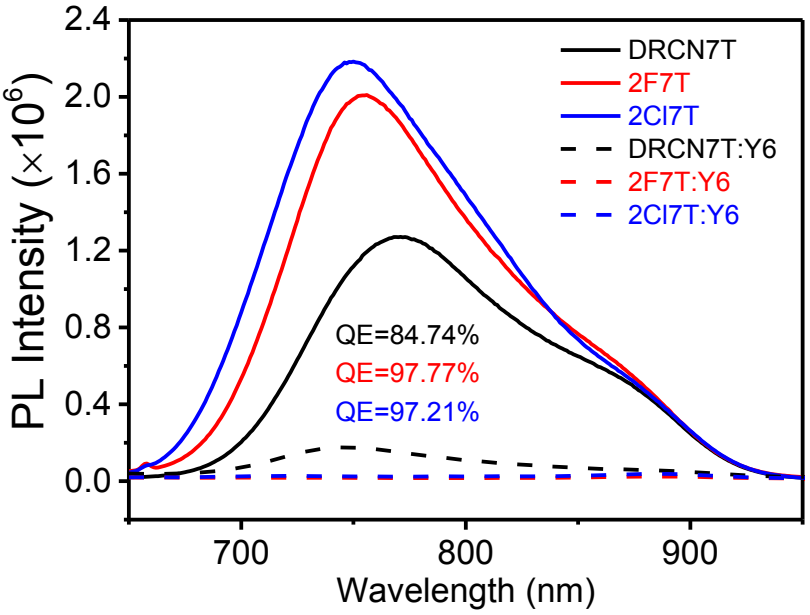

Figure S14. PL spectra of the neat donor films and blend films.

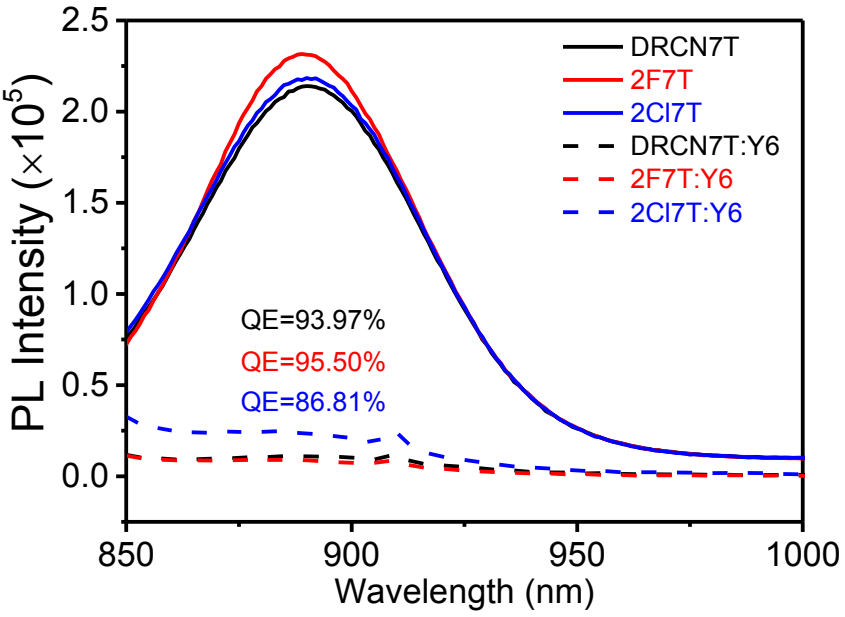

Figure S15. PL spectra of the neat acceptor films and blend films.

15. Grazing-Incidence Wide-Angle X-ray Scattering (GIWAXS)

Grazing-Incidence wide-angle X-ray scattering (GIWAXS) measurements were performed at 5A beamline of the Pohang Light Source II (PLS-II) in Korea. The GIWAXS images were recorded with X-rays of 11.57 keV (λ=1.0716Å) at 0.13 incidence angle.

At first glance, the pristine **DRCN7T** and **2Cl7T** films show a distinct first order (010) π-π stacking peaks in the q_z direction ($d_{(010)}$ = 3.63 and 3.65 Å, respectively) and up to third order (300) scattering peak along both q_{xy} and q_z direction (lamellar spacing ranging from 18.81 to 19.03 Å), indicating they have highly ordered "face-on" dominated bimodal orientation (Figure 5a and c). In contrast, **2F7T** film exhibits a predominant "edge-on" orientation, confirmed by the presence of third order lamellar scattering peaks along q_z direction and (010) refection along q_{xy} direction ($d_{(100)}$ = 19.39 Å and $d_{(010)}$ = 3.61 Å, respectively) (Figure 5b). Among the SMs, **2F7T** having higher crystallinity than other counterparts as substantiated by its shorter π-π stacking distance and higher crystal coherence length of the 010 peak (CCL_{010} = 32.86, 69.86 and 37.43 Å for **DRCN7T**, **2F7T** and **2Cl7T**, respectively) (Table S14).

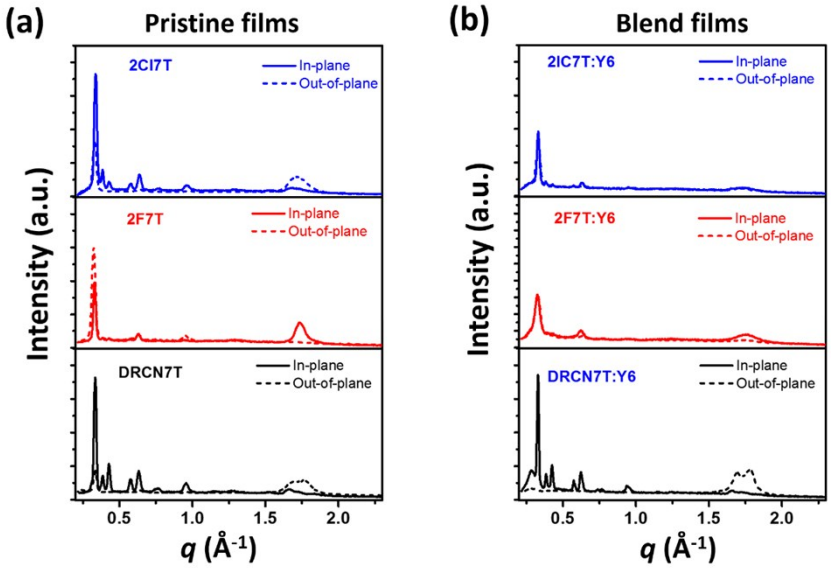

Figure S16. In-plane (q_{xy}, solid line) line cut profiles and out-of-plane (q_{xy}, dotted line) line cut profiles and of the GIWAXS images obtained from pristine SMs and SM:Y6 blend films.

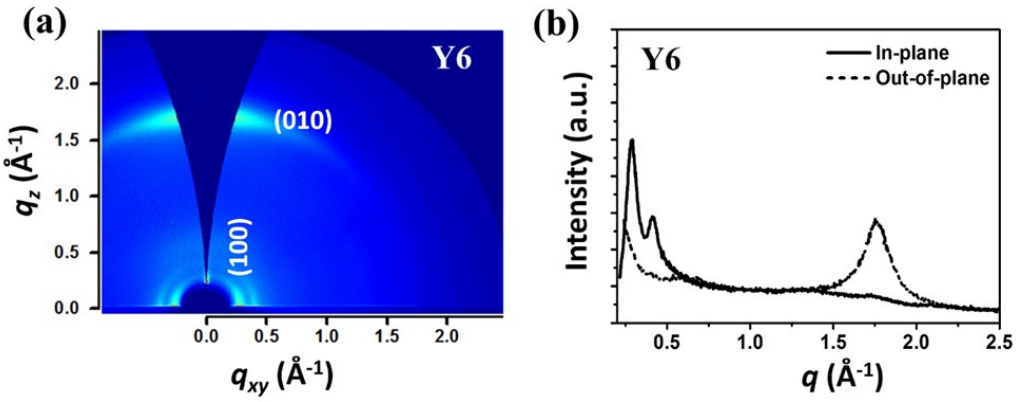

Figure S17. (a) 2D-GIWAXS images of Y6 (b) in-plane (q_{xy}, solid line) line cut profiles and out-of-plane (q_{xy}, dotted line) line cut profiles of the corresponding GIWAXS images.

Table S9. Packing parameters of pristine SMs, as derived from GIWAXS measurements (Fig.5).

Film	OOP [a]			IP [b]		
	***d*-(100) [Å] / (q-(100) [Å^{-1}])**	***d*-(010) [Å] / (q-(010) [Å^{-1}])**	**[c] CCL (Å)$_{010}$**	***d*-(100) [Å] / (q-(100) [Å^{-1}])**	***d*-(010) [Å] / (q-(010) [Å^{-1}])**	**[c] CCL (Å)$_{010}$**
DRCN7T	18.81 (0.334)	3.63 (1.730)	32.86	18.81 (0.334)		
DRCN7T:Y6		3.70 (1.693)	53.71	19.06 (0.329)	**(belonging to DRCN7T)**	
		3.51 (1.786)	68.88	21. 59 (0.291)	**(belonging to Y6)**	
2F7T	19.39 (0.324)			19.02 (0.330)	3.61 (1.738)	69.86
2F7T:Y6	19.20 (0.327)	3.66 (1.712)	33.93	19.29 (0.325)	3.57 (1.755)	30.72
2Cl7T	19.03 (0.330)	3.65 (1.721)	37.43	18.63 (0.337)		
2Cl7T:Y6	19.02 (0.330)	3.64 (1.725)	36.47	18.98 (0.331)	3.55 (1.765)	32.74
Y6		3.56 (1.762)	26.53	21. 86 (0.288)		

[a]Calculation from q_z-axis.

[b]Calculation from q_{xy}-axis.

[c]Calculated from Scherer equation: CCL = $2\pi K/\Delta q$, where Δq is the full-with a half-maximum of the peak and K is a shape factor (0.9 was used here).

16. Solution NMR and HR-MS Spectra

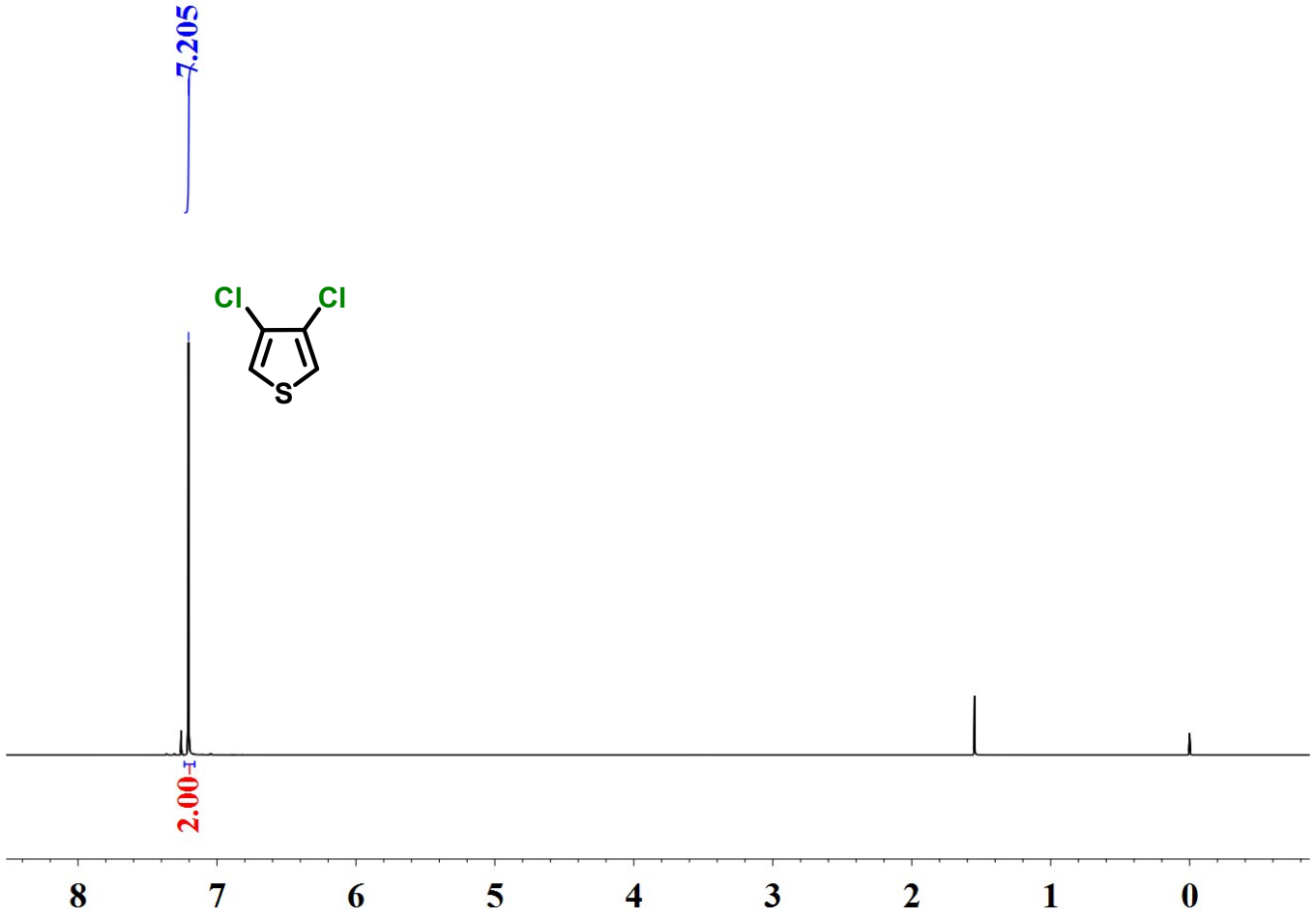

Figure S18. ^{1}H NMR spectrum of **4** in $CDCl_3$.

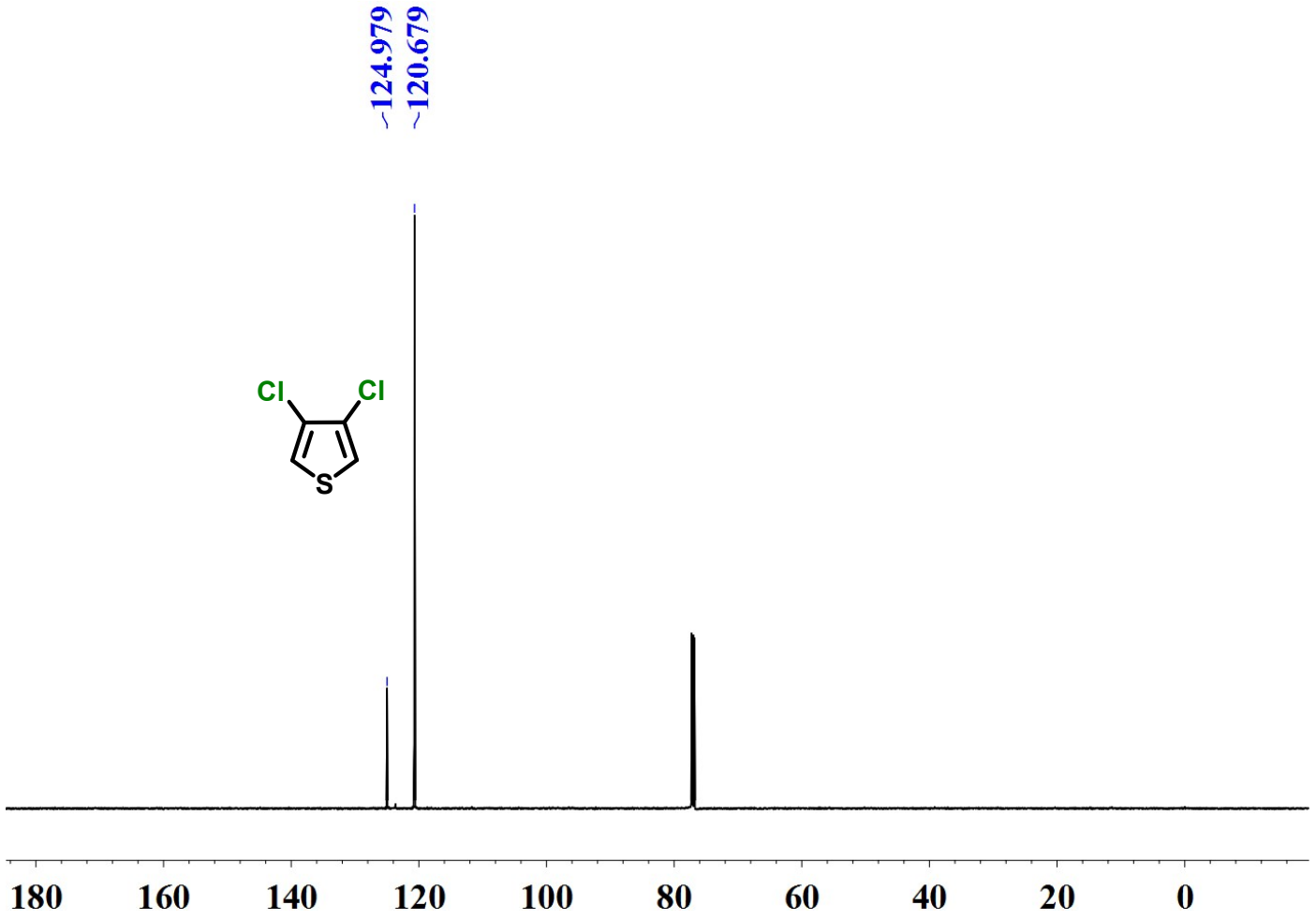

Figure S19. ^{13}C NMR spectrum of **2** in $CDCl_3$.

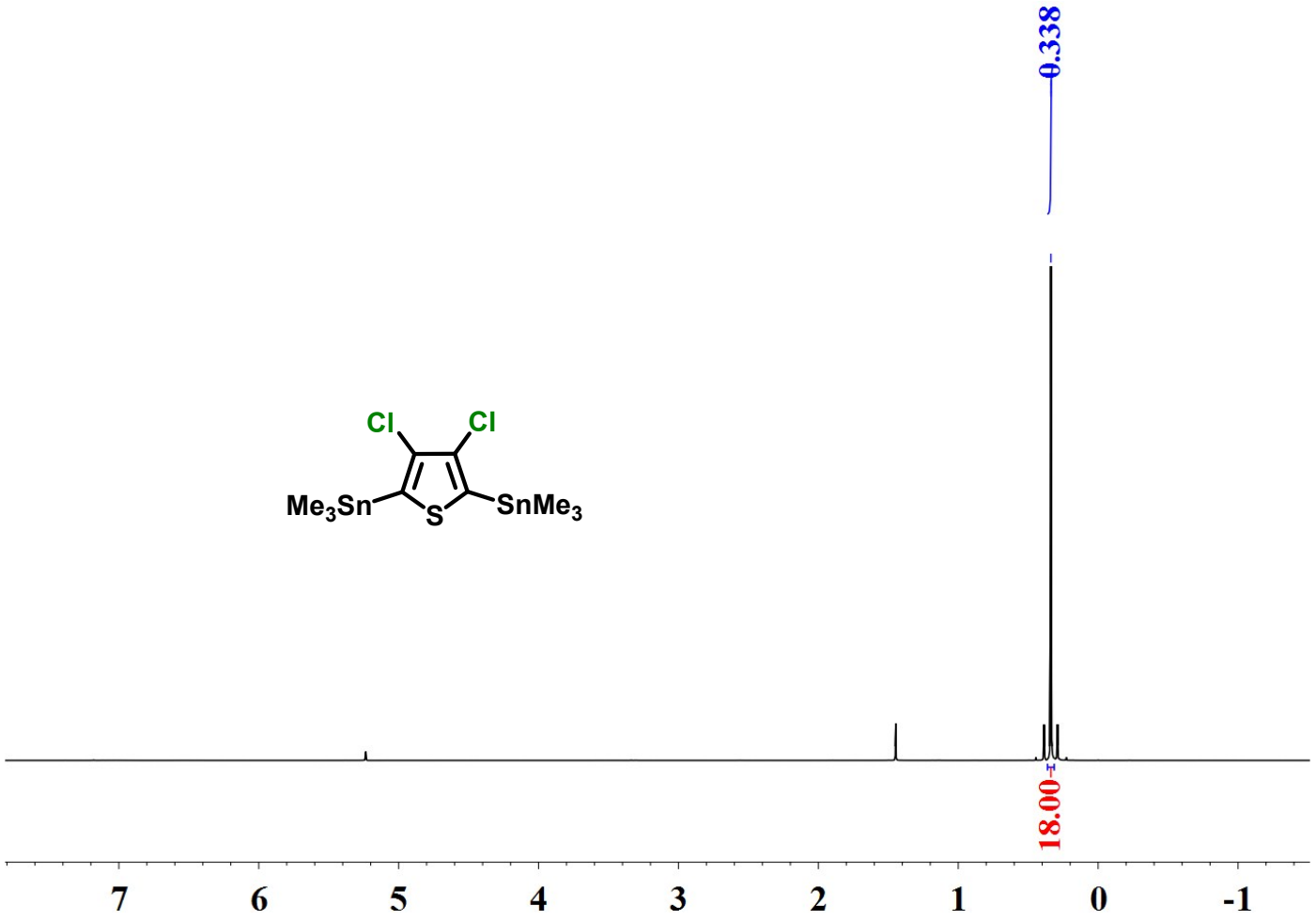

Figure S20. ^{1}H NMR spectrum of **2ClT-Sn** in CD_2Cl_2.

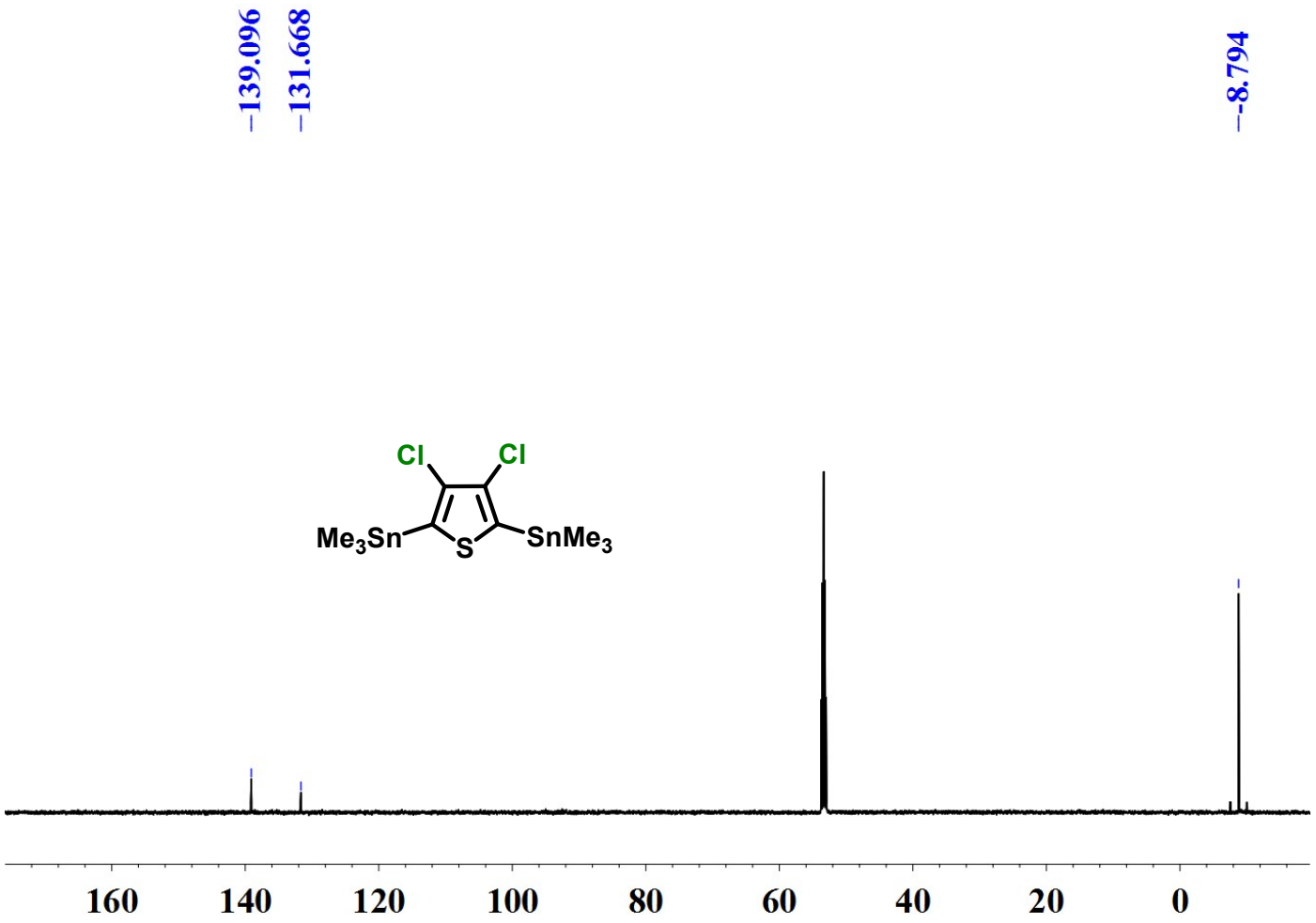

Figure S21. ^{13}C NMR spectrum of **2ClT-Sn** in CD_2Cl_2.

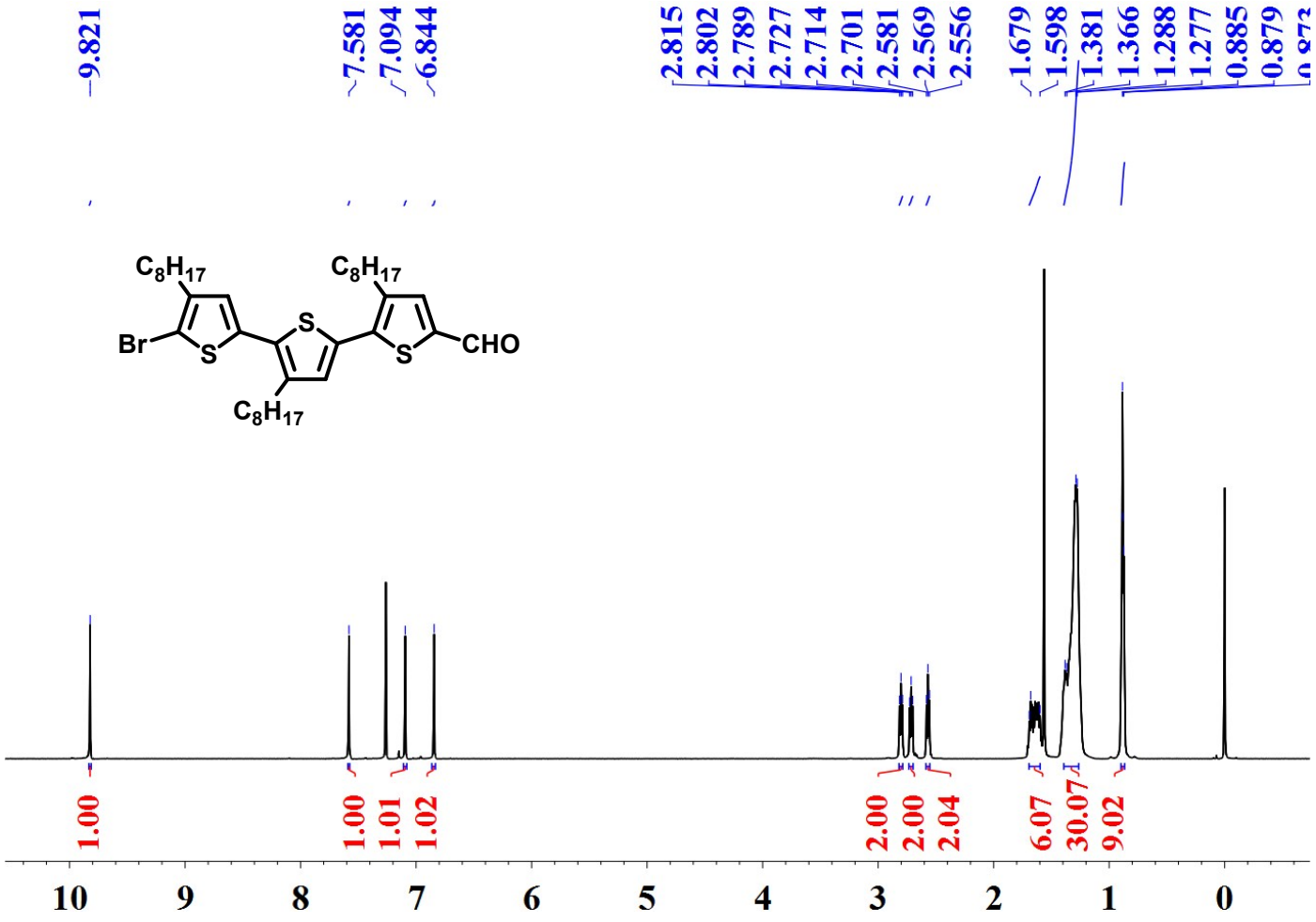

Figure S22. ^{1}H NMR spectrum of **3** in $CDCl_3$.

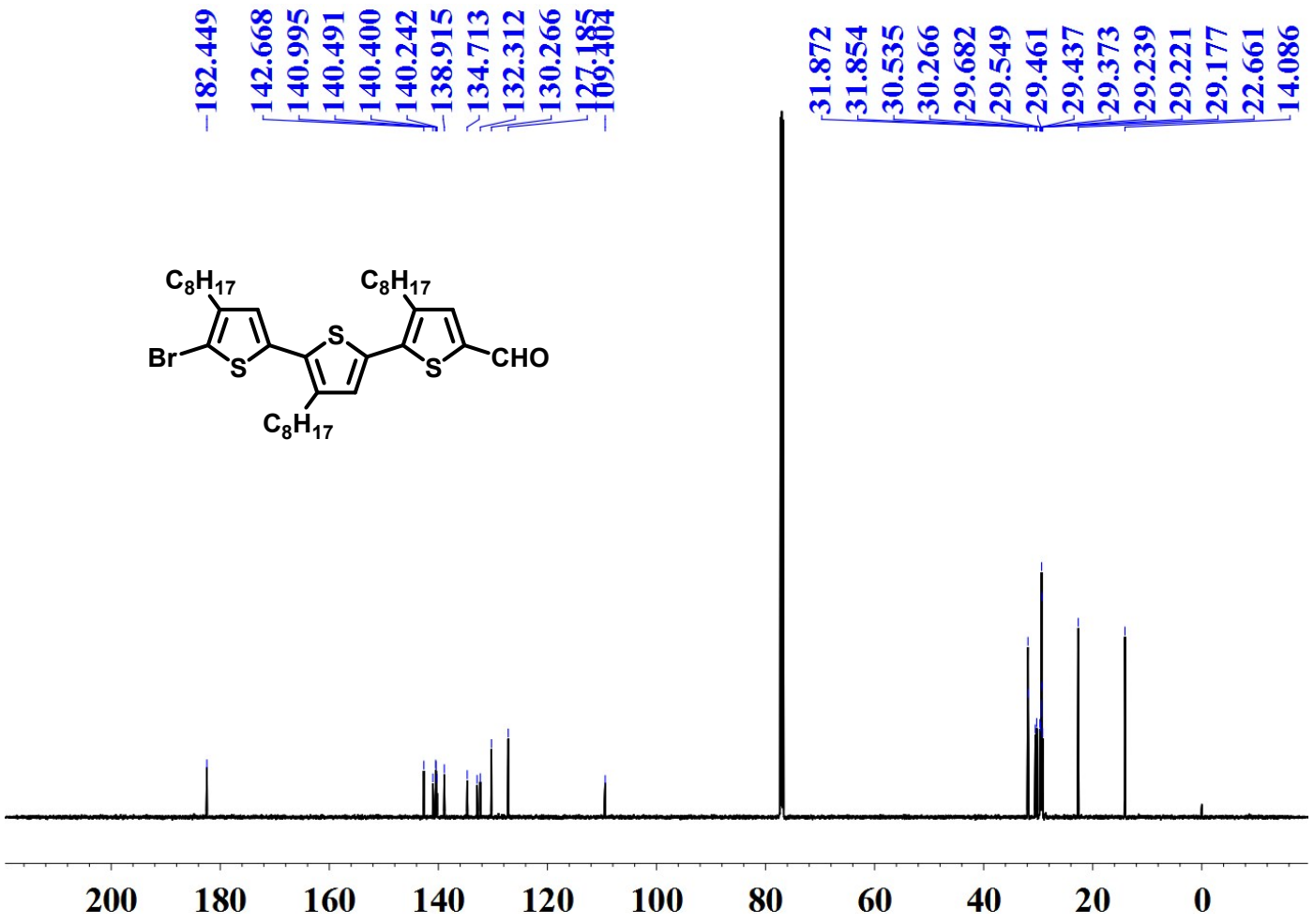

Figure S23. ^{13}C NMR spectrum of **5** in $CDCl_3$.

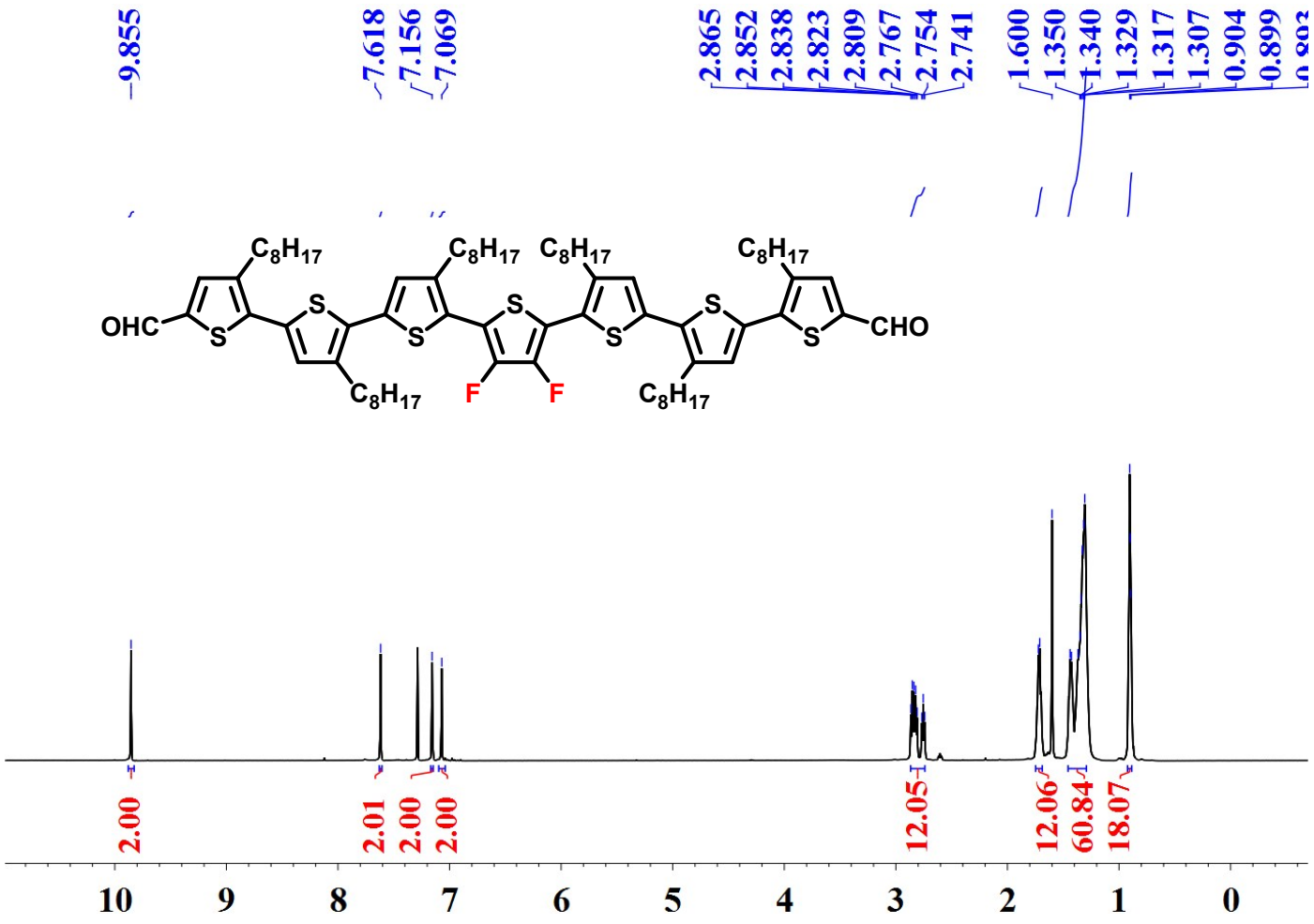

Figure S24. ^{1}H NMR spectrum of **2F7T-CHO** in $CDCl_3$.

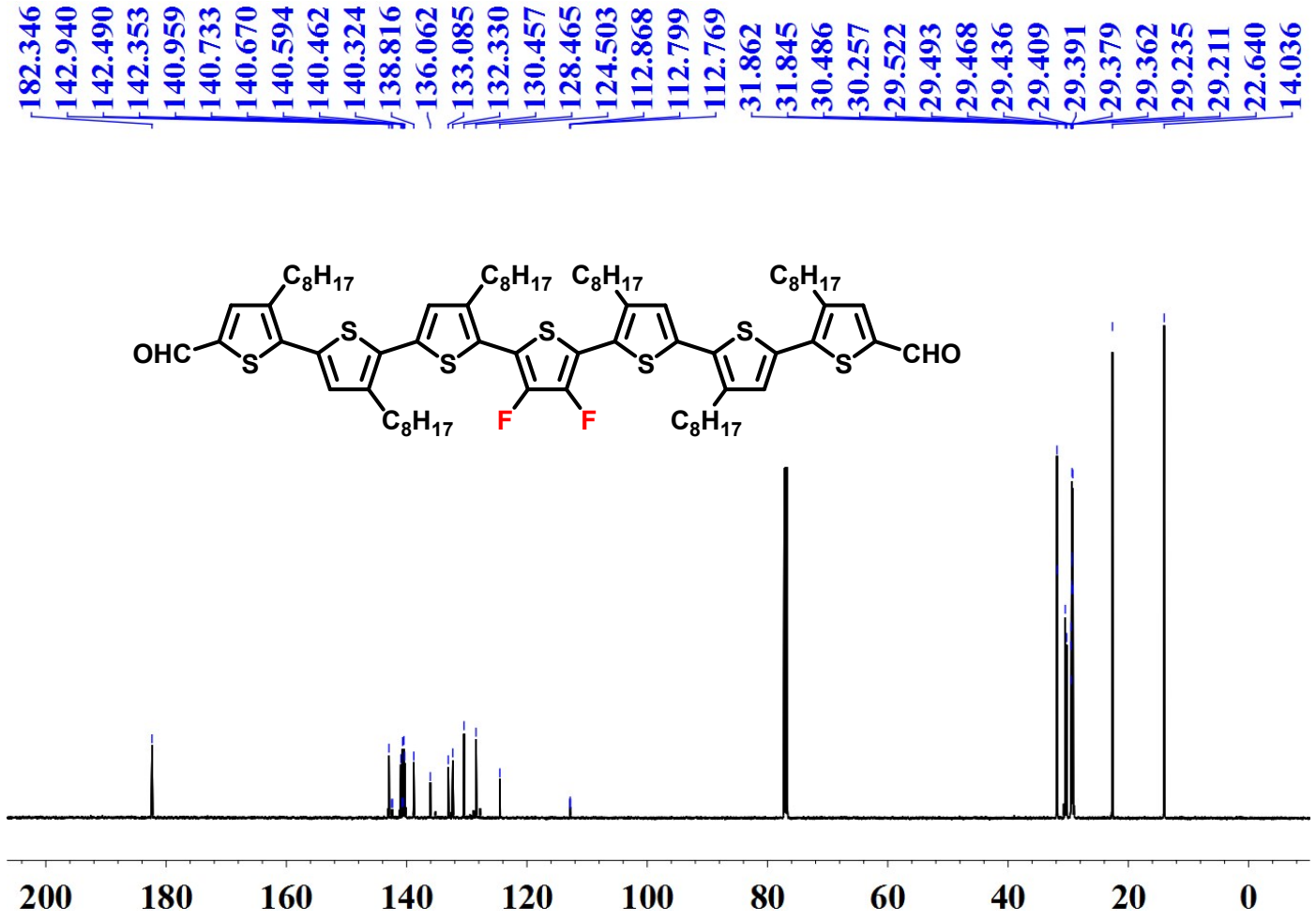

Figure S25. ^{13}C NMR spectrum of **2F7T-CHO** in $CDCl_3$.

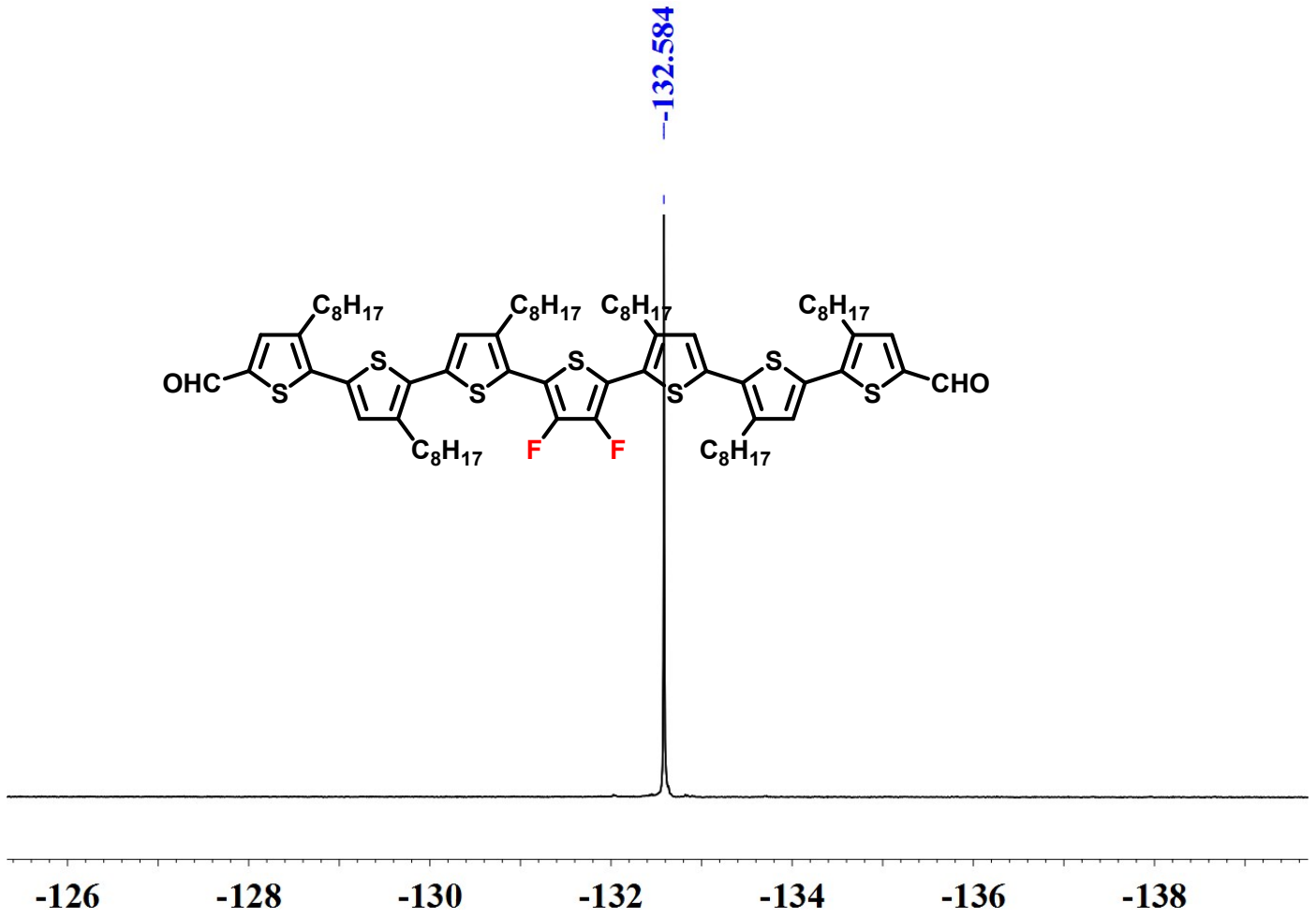

Figure S26. ^{19}F NMR spectrum of **2F7T-CHO** in $CDCl_3$.

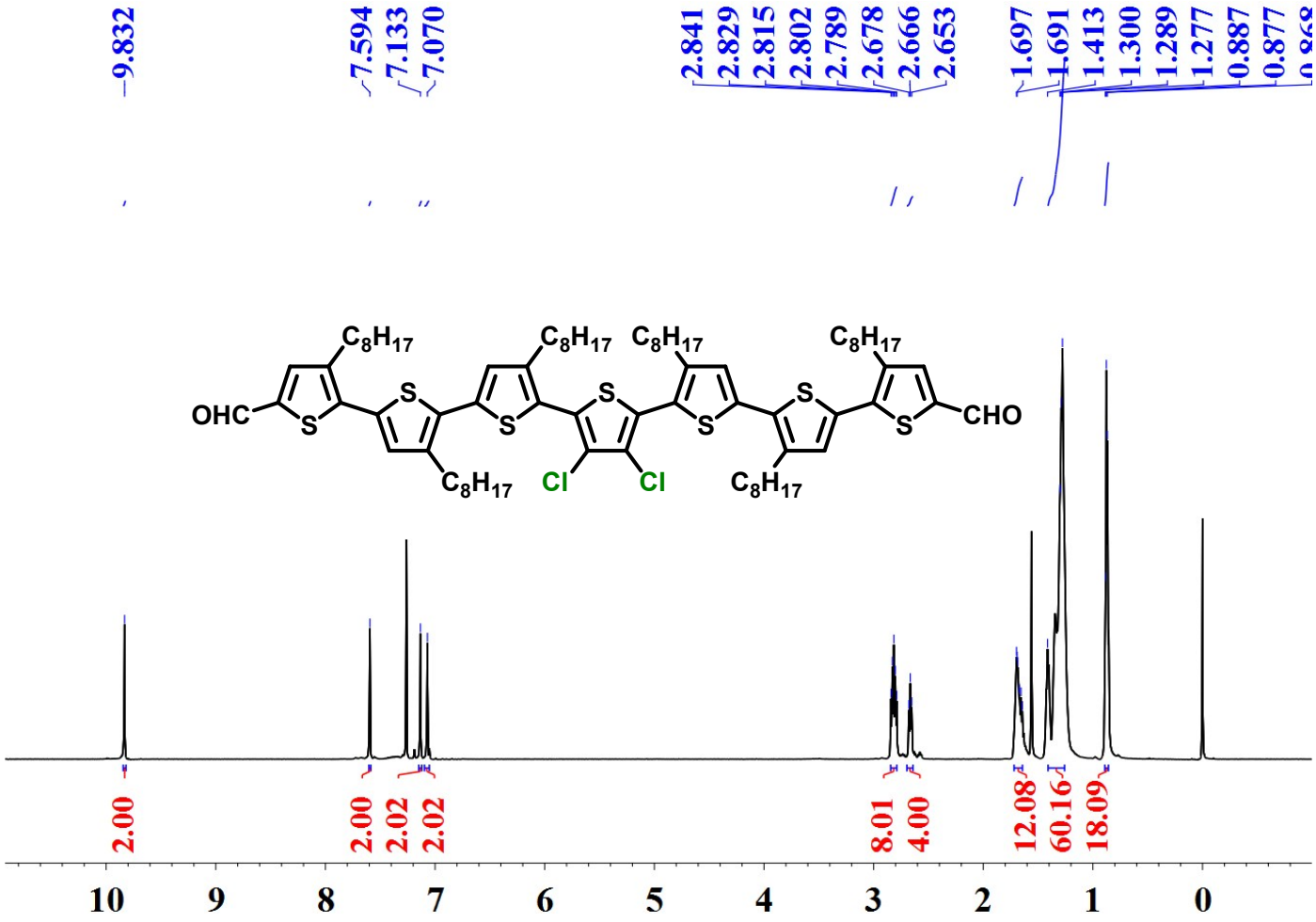

Figure S27. ^{1}H NMR spectrum of **2Cl7T-CHO** in $CDCl_3$.

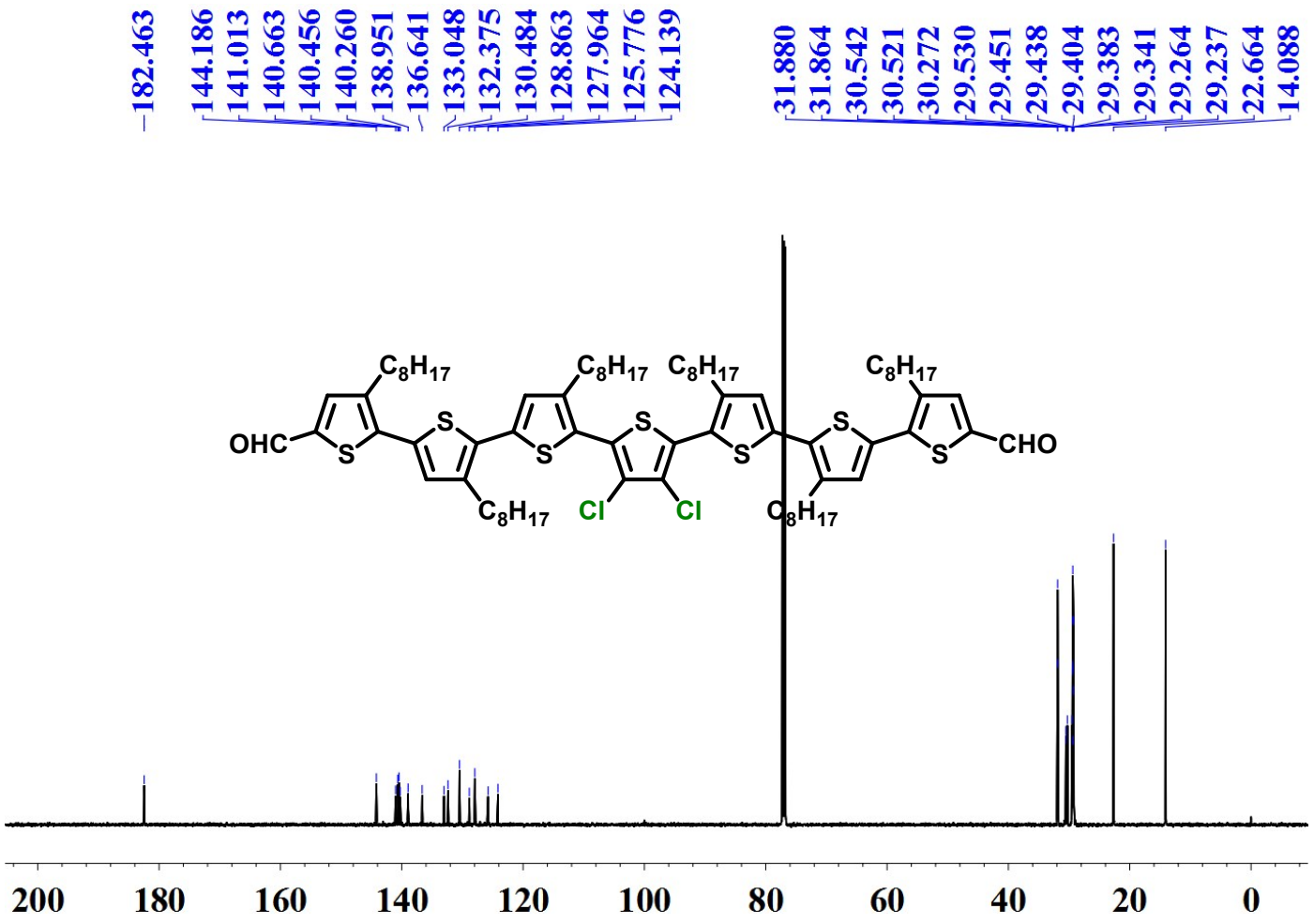

Figure S28. ^{13}C NMR spectrum of **2Cl7T-CHO** in $CDCl_3$.

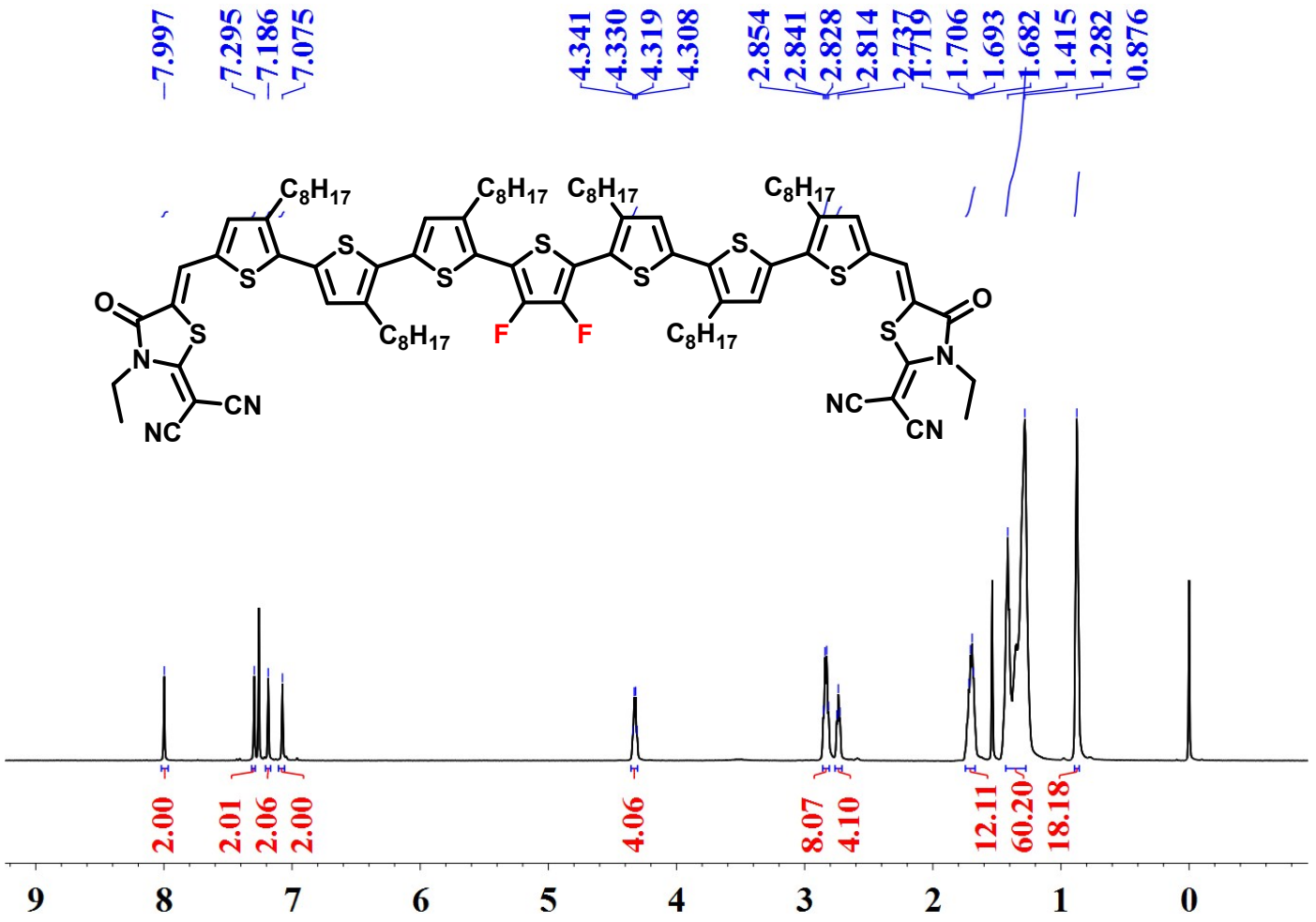

Figure S29. ^{1}H NMR spectrum of **2F7T** in $CDCl_3$.

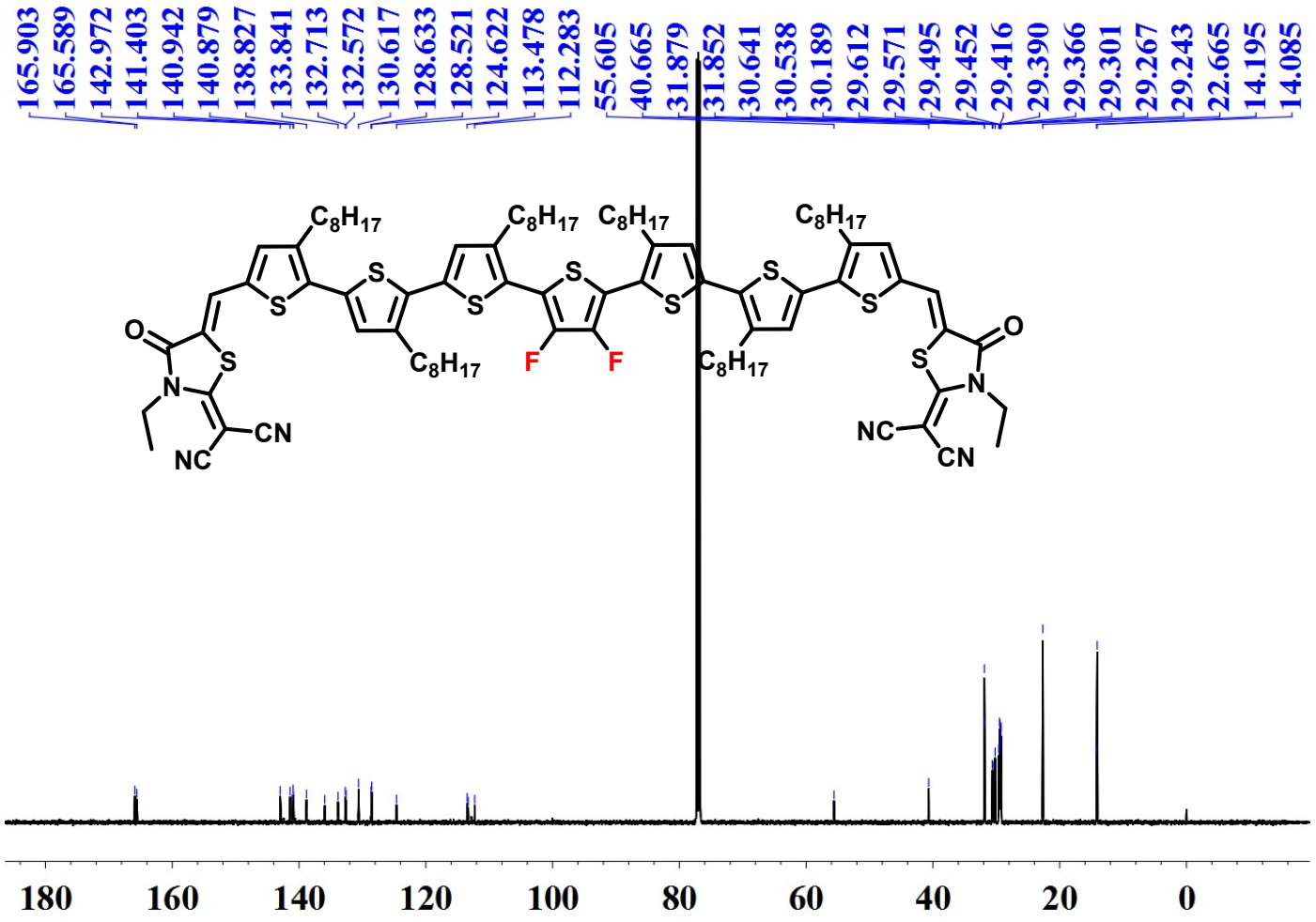

Figure S30. ^{13}C NMR spectrum of **2F7T** in $CDCl_3$.

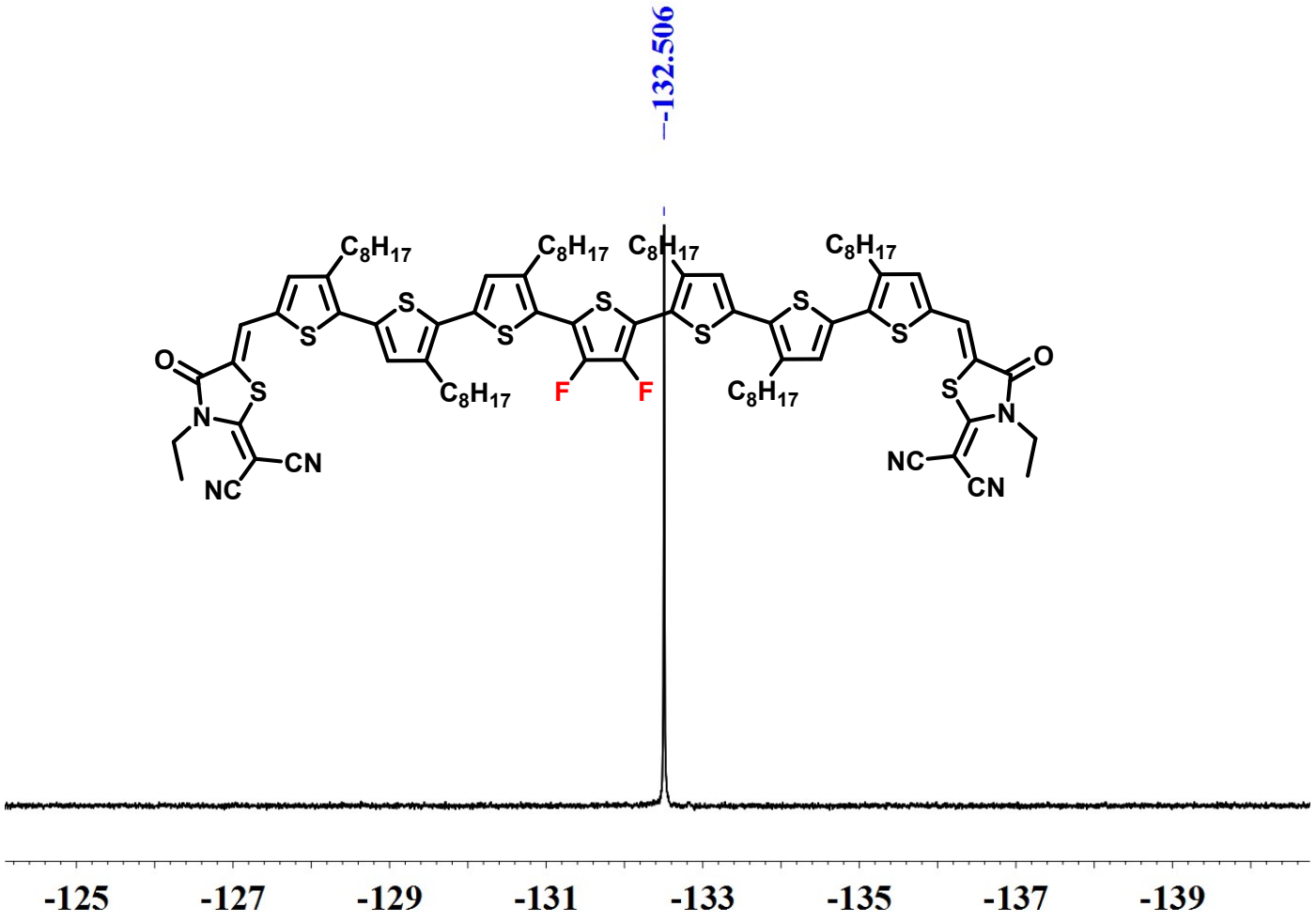

Figure S31. ^{19}F NMR spectrum of **2F7T** in $CDCl_3$.

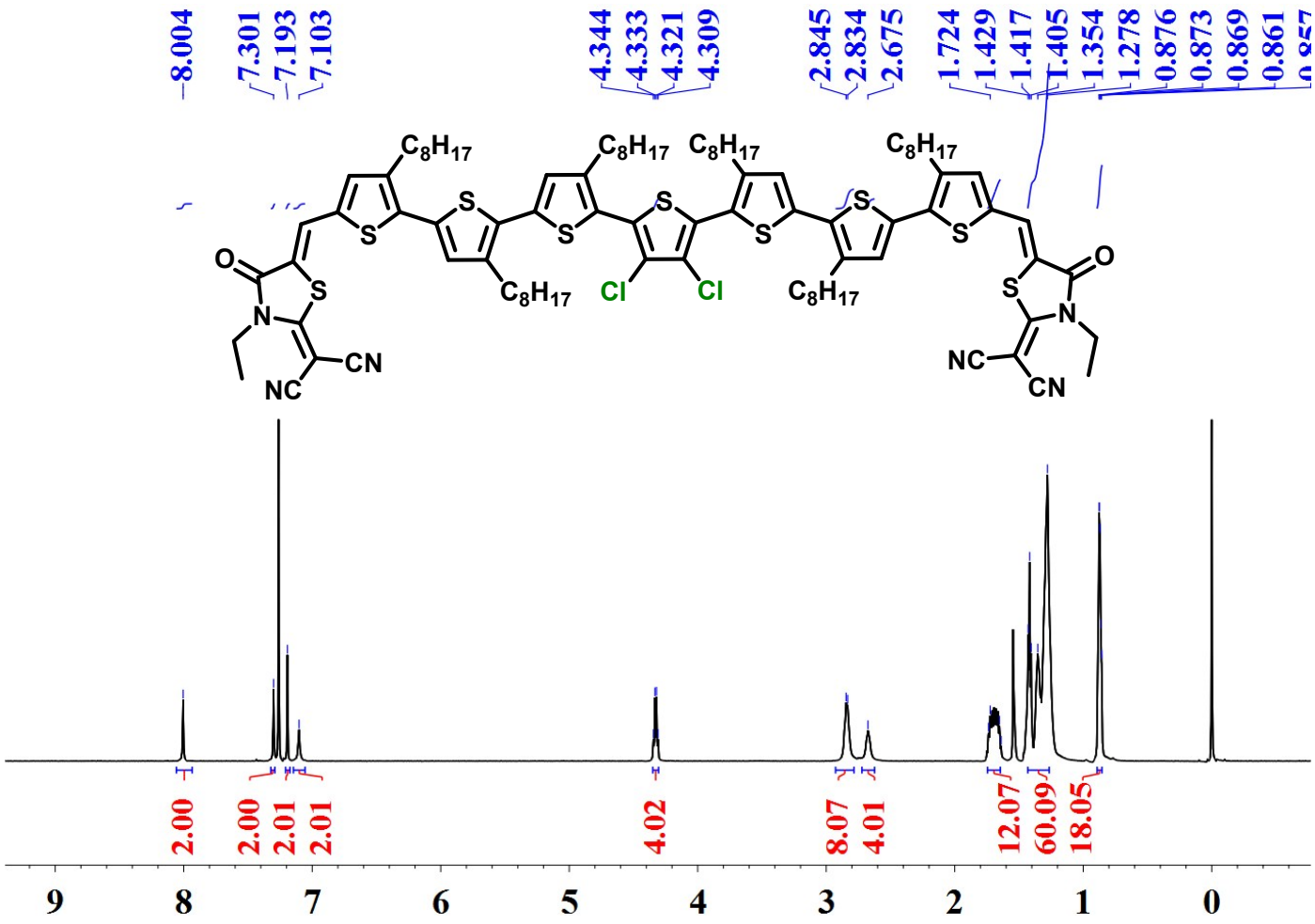

Figure S32. ^{1}H NMR spectrum of **2Cl7T** in $CDCl_3$.

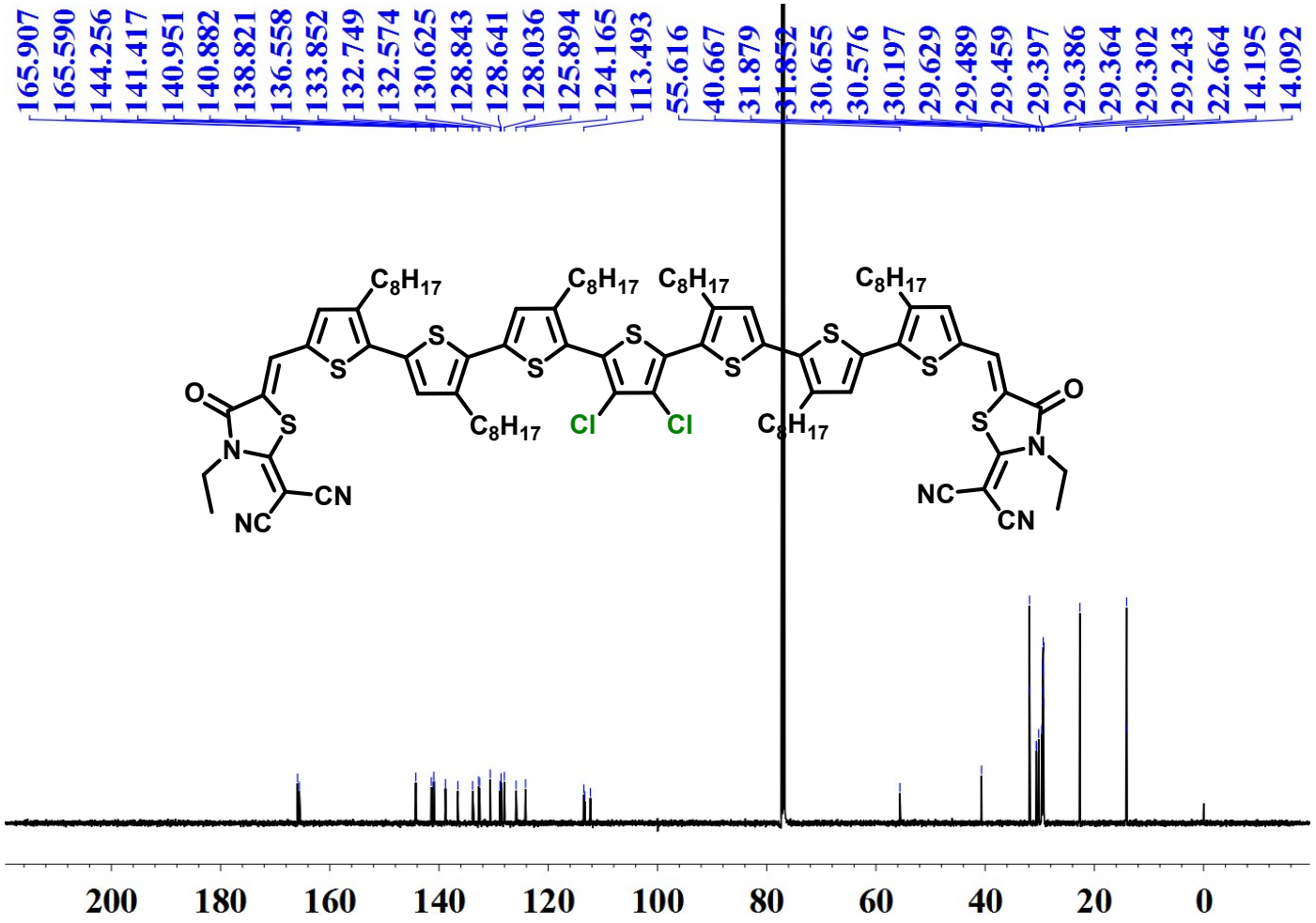

Figure S33. ^{13}C NMR spectrum of **2Cl7T** in $CDCl_3$.

Mass Spectrum List Report

Analysis Info

Analysis Name	D:\Data\HYY\SKD_0_N3_000014.d	Acquisition Date	9/12/2019 10:15:27 PM
Method	5-12-DADOU	Operator	
Sample Name	2018-6-7-MD	Instrument	solariX
Comment	PeptideMix NS=8 TF=1.2		

Acquisition Parameter

Polarity	Positive	n/a	n/a	No. of Laser Shots	100
n/a	n/a	No. of Cell Fills	1	Laser Power	75.0 lp
Broadband Low Mass	53.8 m/z	n/a	n/a	n/a	n/a
Broadband High Mass	3000.0 m/z	n/a	n/a	n/a	n/a
Acquisition Mode	Single MS	n/a	n/a		
Pulse Program	basic	n/a	n/a	Calibration Date	Fri Feb 21 02:36:54 2014
Source Accumulation	0.100 sec	n/a	n/a	Data Acquisition Size	4194304
Ion Accumulation Time	0.500 sec	n/a	n/a	Apodization	Sine-Bell Multiplication
Flight Time to Acq. Cell	0.001 sec	n/a	n/a	Apodization	Apodization

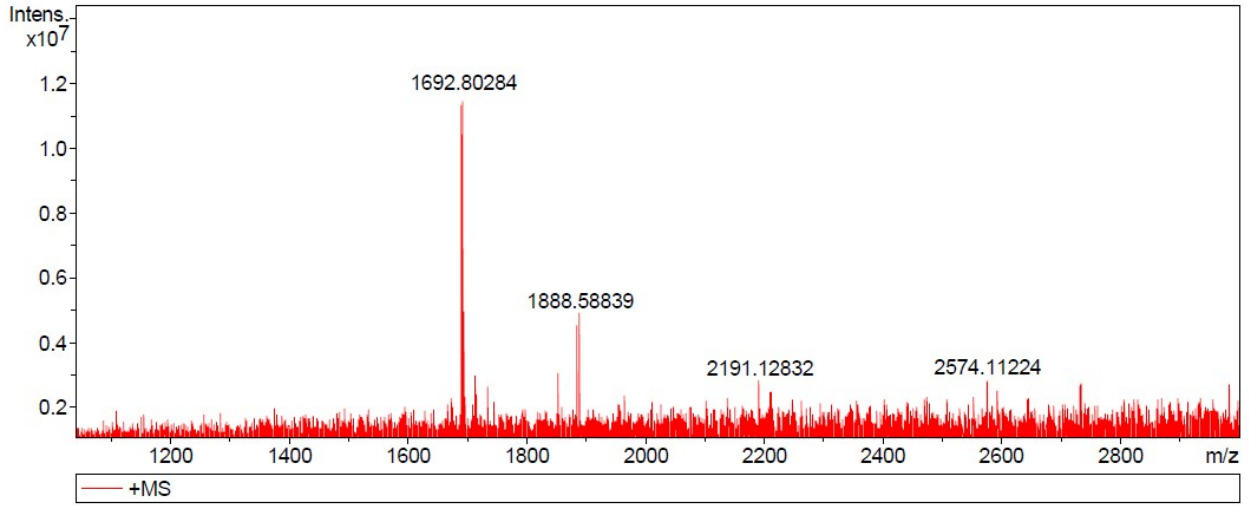

Figure S34. HR-MS spectrum of **2F7T**.

Mass Spectrum List Report

Analysis Info

Analysis Name	D:\Data\HYY\SKD_0_N5_000011.d	Acquisition Date	9/12/2019 10:03:54 PM
Method	5-12-DADOU	Operator	
Sample Name	2018-6-7-MD	Instrument	solariX
Comment	PeptideMix NS=8 TF=1.2		

Acquisition Parameter

Polarity	Positive	n/a	n/a	No. of Laser Shots	100
n/a	n/a	No. of Cell Fills	1	Laser Power	75.0 lp
Broadband Low Mass	53.8 m/z	n/a	n/a	n/a	n/a
Broadband High Mass	3000.0 m/z	n/a	n/a	n/a	n/a
Acquisition Mode	Single MS	n/a	n/a		
Pulse Program	basic	n/a	n/a	Calibration Date	Fri Feb 21 02:36:54 2014
Source Accumulation	0.100 sec	n/a	n/a	Data Acquisition Size	4194304
Ion Accumulation Time	0.500 sec	n/a	n/a	Apodization	Sine-Bell Multiplication
Flight Time to Acq. Cell	0.001 sec	n/a	n/a	Apodization	Apodization

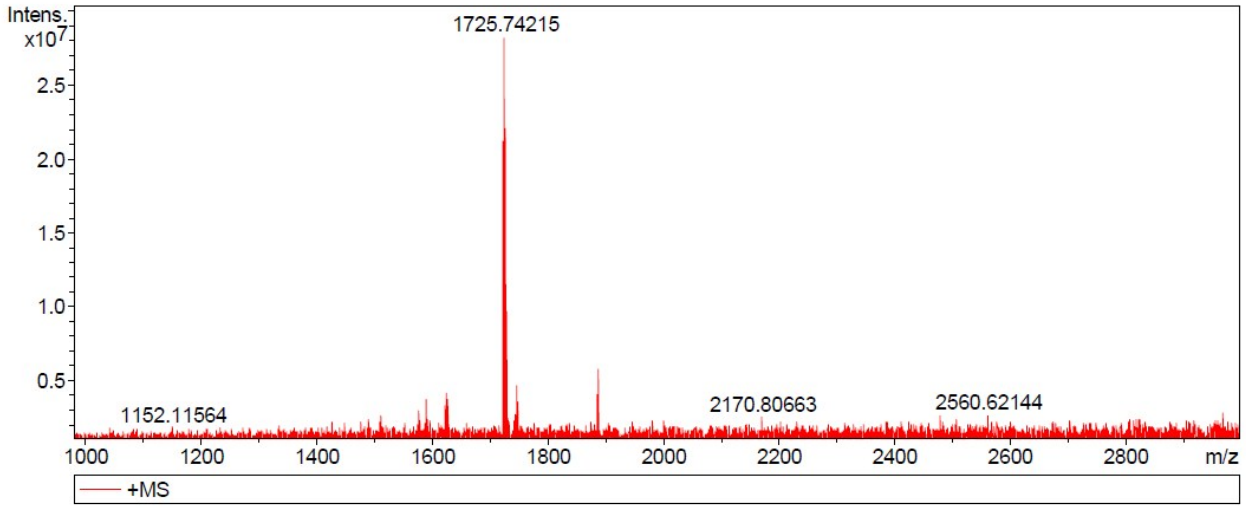

Figure S34. HR-MS spectrum of **2Cl7T**.

17. References

[1] S.J. Liu, P. Boufflet, S. Wood, J. Wade, J. Moriarty, E. Gann, E. L. Ratcliff, C. R. McNeill, H. Sirringhaus, J. S. Kim, M. Heeney, *J. Am. Chem. Soc.*, 2015, **137**, 6866-6879.

[2] Y. S. Liu, X. J. Wan, F. Wang, J. Y. Zhou, G. K. Long, J. G. Tian, Y. S. Chen, *Adv. Mater.* **2011**, *23*, 5387-5391.

[3] J. Pommerehne, H. Vestweber, W. Guss, R. F. Mahrt, H. Bassler, M. Porsch, J. Daub, *Adv. Mater.* **1995**, *7*, 551-554.

[4] J. C. Blakesley, F. A. Castro, W. Kylberg, G. F. A. Dibb, C. Arantes, R. Valaski, M. Cremona, J. S. Kim, J.-S. Kim, *Organic Electronics* **2014**, *15*, 1263-1272.